J Physiol 587.7 (2009) pp 1439–1459

The Journal of Physiology

Inositol-1,4,5-trisphosphate receptor-mediated Ca^{2+} waves in pyramidal neuron dendrites propagate through hot spots and cold spots

John S. Fitzpatrick[1], Anna M. Hagenston[1], Daniel N. Hertle[1], Keith E. Gipson[1], Lisa Bertetto-D'Angelo[1] and Mark F. Yeckel[1,2]

[1]*Department of Neurobiology and* [2]*The Kavli Institute for Neuroscience, Yale University School of Medicine*

We studied inositol-1,4,5-trisphosphate (IP_3) receptor-dependent intracellular Ca^{2+} waves in CA1 hippocampal and layer V medial prefrontal cortical pyramidal neurons using whole-cell patch-clamp recordings and Ca^{2+} fluorescence imaging. We observed that Ca^{2+} waves propagate in a saltatory manner through dendritic regions where increases in the intracellular concentration of Ca^{2+} ($[Ca^{2+}]_i$) were large and fast ('hot spots') separated by regions where increases in $[Ca^{2+}]_i$ were comparatively small and slow ('cold spots'). We also observed that Ca^{2+} waves typically initiate in hot spots and terminate in cold spots, and that most hot spots, but few cold spots, are located at dendritic branch points. Using immunohistochemistry, we found that IP_3 receptors (IP_3Rs) are distributed in clusters along pyramidal neuron dendrites and that the distribution of inter-cluster distances is nearly identical to the distribution of inter-hot spot distances. These findings support the hypothesis that the dendritic locations of Ca^{2+} wave hot spots in general, and branch points in particular, are specially equipped for regenerative IP_3R-dependent internal Ca^{2+} release. Functionally, the observation that IP_3R-dependent $[Ca^{2+}]_i$ rises are greater at branch points raises the possibility that this novel Ca^{2+} signal may be important for the regulation of Ca^{2+}-dependent processes in these locations. Futhermore, the observation that Ca^{2+} waves tend to fail between hot spots raises the possibility that influences on Ca^{2+} wave propagation may determine the degree of functional association between distinct Ca^{2+}-sensitive dendritic domains.

(Resubmitted 9 January 2009; accepted 3 February 2009; first published online 9 February 2009)

Corresponding author M. F. Yeckel: Department of Neurobiology, Yale University School of Medicine, 333 Cedar St, New Haven, CT 06510, USA. Email: mark.yeckel@yale.edu

Rises in $[Ca^{2+}]_i$ participate in a vast array of signalling events in virtually all cell types. Despite the ubiquitous nature of Ca^{2+}, this second messenger can nonetheless elicit highly specific responses that depend both on the location and the magnitude of the $[Ca^{2+}]_i$ rise (Berridge, 1997; Berridge, 1998; Rose & Konnerth, 2001). This is particularly evident in neurons, which have a complex and compartmentalized structure. For example, rises in $[Ca^{2+}]_i$ have been shown to have profoundly different consequences on neuronal function depending on whether those rises occur in neuron somata, proximal dendrites, distal dendrites, dendritic branch points, or dendritic spines. Thus, it is important to know what determines the spatial distribution of $[Ca^{2+}]_i$ rises in neurons, and particularly within their dendrites.

Increases in $[Ca^{2+}]_i$ within dendrites may be mediated by a number of different mechanisms. Ca^{2+} can enter dendritic structures from the extracellular space via voltage-gated Ca^{2+} channels (VGCCs) or ligand-gated channels, and Ca^{2+} can enter the dendritic cytosol when it is released from intracellular stores such as the endoplasmic reticulum (ER). Internal Ca^{2+} release in pyramidal neurons is triggered by activation of neurotransmitter receptors coupled to $G_{q/11}$ and $G_{i/o}$ proteins, which in turn initiate a signalling cascade that leads to mobilization of IP_3. Once initiated, internal Ca^{2+} release can propagate as a wave through the dendritic tree (Jaffe & Brown, 1994). Internal Ca^{2+} release and Ca^{2+} waves triggered by stimulation of synaptic afferents have been observed in pyramidal neurons from several neural regions, including hippocampal areas CA3 (Pozzo-Miller

J. S. Fitzpatrick and A. M. Hagenston contributed equally to this work and are listed alphabetically.

DOI: 10.1113/jphysiol.2009.168930

et al. 1996; Yeckel *et al.* 1999; Kapur *et al.* 2001) and CA1 (Nakamura *et al.* 1999; Gipson & Yeckel, 2007), medial prefrontal cortex (Hagenston *et al.* 2008), somatosensory cortex (Larkum *et al.* 2003) and basolateral amygdala (Power & Sah, 2005), as well as in dopaminergic neurons of the midbrain (Morikawa *et al.* 2003).

Although relatively little is known about the mechanisms underlying Ca^{2+} wave propagation in neurons, Ca^{2+} waves have been extensively studied in many non-neuronal cell types, including HeLa cells, *Xenopus* oocytes, cardiac myocytes, and astrocytes (Yagodin *et al.* 1994; Cheng *et al.* 1996; Bootman *et al.* 1997; Sheppard *et al.* 1997; Callamaras *et al.* 1998). In these cells, Ca^{2+} is released from the ER at discrete spatial locations (Parker & Ivorra, 1990; Yao *et al.* 1995; Bootman *et al.* 1997; Sun *et al.* 1998). Liberation of Ca^{2+} at these release sites may be triggered either in isolation or in conjunction with the generation of propagating Ca^{2+} waves (Cheng *et al.* 1993; Yagodin *et al.* 1994; Callamaras *et al.* 1998). More specifically, internal Ca^{2+} release is thought to propagate between release sites only when the local concentration of Ca^{2+} that has diffused away from one such site is sufficiently large to stimulate release at neighbouring sites (Yagodin *et al.* 1994; Wang & Thompson, 1995; Berridge, 1997; Bootman *et al.* 1997; Callamaras *et al.* 1998). The generation of propagating Ca^{2+} waves also depends on the intracellular concentration of IP_3 ($[IP_3]_i$) produced in response to stimulation. When $[IP_3]_i$ is well above the threshold for release, the amount of Ca^{2+} mobilized at each individual site is large. Under these conditions, the delay as Ca^{2+} diffuses between release sites is brief and the wave appears continuous. By contrast, when $[IP_3]_i$ lies only slightly above release threshold, less Ca^{2+} is liberated at each site and the delay as Ca^{2+} diffuses between adjacent sites is large. The Ca^{2+} waves generated under these conditions appear to propagate in a saltatory fashion (Yagodin *et al.* 1994; Bootman *et al.* 1997; Callamaras *et al.* 1998). Ca^{2+} wave initiation and propagation in non-neuronal cells may thus be best understood in terms of a 'fire-diffuse-fire' model of intracellular Ca^{2+} release (Keizer *et al.* 1995; Pearson & Ponce-Dawson, 1998; Dawson *et al.* 1999). According to this model, Ca^{2+} initially liberated from one or many strongly activated release site(s) may diffuse to and stimulate neighbouring sites, which might subsequently release Ca^{2+} that diffuses to yet more release sites, and so on (Parker *et al.* 1996; Bootman *et al.* 1997).

In this study, we examined the properties of dendritic Ca^{2+} waves in CA1 hippocampal and layer V medial prefrontal cortical pyramidal neurons. We found that these Ca^{2+} waves propagated non-uniformly between locations in which both the amplitudes of $[Ca^{2+}]_i$ rises and the rates at which $[Ca^{2+}]_i$ rose were consistently greater ('hot spots'), and through locations in which the amplitudes and rates of rise of Ca^{2+} release were consistently smaller ('cold spots'). Our data indicate that hot spots are predominantly located at dendritic branch points, and that Ca^{2+} waves tend to initiate in hot spots and fail in the regions of dendrite between them. Using immunohistochemistry, we show that IP_3Rs, which comprise an integral component of the Ca^{2+} release machinery in pyramidal neurons, form clusters along these cells' dendrites and at their dendritic branch points. These observations support the hypothesis that Ca^{2+} waves in pyramidal neurons propagate via a fire-diffuse-fire mechanism between regions enriched for IP_3Rs. We propose that the larger amplitude $[Ca^{2+}]_i$ rises observed in hot spots may be particularly important for the regulation of Ca^{2+}-dependent processes at dendritic branch points, and may thus participate in the integration of synaptic signals arriving on oblique dendrites. We additionally suggest that factors which limit or enhance the propagation of Ca^{2+} waves through cold spots may regulate the extent of functional segregation between the dendritic domains that these cold spots define.

Methods

All experimental procedures were approved by the Institutional Animal Care and Use Committee at Yale University School of Medicine, and are consistent with procedures outlined in *Guidelines for the Care and Use of Mammals in Neuroscience and Behavioral Research* (The National Academies Institute for Laboratory Animal Research, 2003) and the *2000 Report of the AVMA Panel on Euthanasia* (AVMA Panel on Euthanasia. American Veterinary Medical Association, 2001).

Slice preparation

Brain slices were prepared from postnatal days (P) 21–58 male Sprague–Dawley rats ($n = 49$ animals; mean age = P28; 4 animals > P41) or 7- to 14-week-old ferrets ($n = 2$ animals). Animals were deeply anaesthetized by intraperitoneal injection of either a ketamine–xylazine–acepromazine mixture (rats) or sodium pentobarbital (ferrets) and decapitated when no longer responsive to a foot pinch. P35–P58 rats were perfused transcanially with ice-cold slicing artificial cerebrospinal fluid (ACSF) prior to decapitation. Following decapitation, brains were quickly removed, blocked and glued to the stage of a Vibratome 1500 or Vibratome 3000, and submerged in 1–3°C slicing ACSF containing (in mM) NaCl (87), KCl (2.5), $CaCl_2$ (0.5), $MgCl_2$ (7), NaH_2PO_4 (1.25), $NaHCO_3$ (25), dextrose (10) and sucrose (75). Slices were cut 320–400 μm thick, incubated in slicing ACSF for 10–20 min at 34–37°C, then transferred to 34–37°C recording ACSF containing (in mM) NaCl (124), KCl (2.5), $CaCl_2$ (2), $MgCl_2$ (2), NaH_2PO_4 (1.25), $NaHCO_3$ (25) and dextrose (10), and allowed to recover for at

least 1 h at room temperature prior to recordings. In some experiments, as indicated, the recording ACSF included the ionotropic γ-amino-butyric acid (GABA) receptor antagonist gabazine (50 μM), the metabotropic GABA receptor antagonist CGP55845 (1 μM), the amino-3-hydroxy-5-methyl-4-isoxazolepropionic acid (AMPA) receptor antagonist dinitroquinoxaline (20 μM), and the NMDA receptor co-agonist glycine (10 μM) in the presence of 0 mM extracellular magnesium (Mg^{2+}) or the NMDA receptor antagonist D,L-2-amino-5-phosphonovaleric acid (D,L-APV; 100 μM) in the presence of high divalent ions (4 mM Ca^{2+} and 5 mM Mg^{2+}; Gipson & Yeckel, 2007). Two cells included in this study were obtained from 7- to 14-week-old ferrets ($n = 2$ animals). In our experience, IP_3R-mediated internal Ca^{2+} release and Ca^{2+} waves in ferret pyramidal neurons are qualitatively indistinguishable from those in rat pyramidal neurons (Hagenston *et al.* 2008). The data obtained from ferret cells were therefore pooled with those obtained from rat cells.

Data collection

Pyramidal neurons in area CA1 of the hippocampus and layer V of the medial prefrontal cortex were visualized using an upright microscope with infrared differential interference contrast optics and recorded using the whole-cell patch-clamp technique. Recording pipettes (3–5 MΩ) were filled with (in mM) KCH_3SO_4 (134), Hepes (10), $MgCl_2$ (1), KCl (3), Mg-ATP (4), Na-GTP (0.5), disodium creatine phosphate salt (5), dipotassium creatine phosphate salt (5) and creatine phosphokinase (50 units ml^{-1}), as well as 15 μM Alexa 488 or 5 μM Alexa 568 for visualization of filled processes, and one of the following Ca^{2+} indicator dyes to monitor changes in $[Ca^{2+}]_i$: 100 μM bis-fura-2, 200 μM fura-2FF or 100 μM fluo-4 (Invitrogen/Molecular Probes, Eugene, OR, USA). For uncaging experiments, the intracellular solution was supplemented with 97 μM 1-(2-nitro-phenyl)ethyl (NPE)-caged IP_3 (Calbiochem/EMD Biosciences, San Diego, CA, USA).

Stimulation

Synaptic responses were evoked with one or two bipolar electrodes constructed from an ACSF-filled broken patch pipette (5–10 μm diameter tip) with a tungsten rod (100 μm diameter; A-M Systems, Carlsborg, WA, USA) glued to its side. In hippocampal slices, stimulating electrodes were placed in stratum radiatum 50–100 μm away from stratum pyramidale and ∼50 μm from the primary apical dendrite of the recorded cell. In medial prefrontal cortical slices, the stimulating electrode was positioned 20–60 μm away from the cell soma and 20–50 μm from the primary apical dendrite of the recorded cell. Stimulation intensities ranged from 5 to 100 μA. Bis-fura-2 and fura-2FF were excited with ∼380 nm radiation from a xenon arc lamp (Opti-Quip, Highland Mills, NY, USA), and the emitted light (490–530 nm) was detected using a cooled CCD camera (Roper Photometrics Quantix 57, Tucson, AZ, USA) at 50 frames s^{-1}. Fluo-4 excitation and emission wavelengths were ∼488 nm and ∼515 nm, respectively. Electrical signals were amplified (npi SEC-05LX, Tamm, Germany), filtered (2 kHz low-pass), and sampled at 10 kHz (Instrutech ITC-18, Port Washington, NY, USA). Data collection and analysis were carried out using custom software developed in Igor Pro (Wavemetrics, Lake Oswego, OR, USA). For focal agonist application, a 3–6 MΩ pipette was filled with the group I/II metabotropic glutamate receptor (mGluR) agonist (±)-1-aminocyclopentane-*trans*-1,3-dicarboxylic acid (ACPD, 400 μM; Tocris Bioscience; Ellisville, MO, USA) in standard recording ACSF or in recording ACSF where 10 mM Hepes replaced 10 mM dextrose, and positioned ∼50 μm away from the soma and < 10 μm from the primary apical dendrite of the recorded cell. Photolysis of NPE-caged IP_3 over an area ∼20 μm in diameter was accomplished as previously described (Hagenston *et al.* 2008). When stimulation failed to trigger a Ca^{2+} wave, the neuron was 'primed' for release by a 5–10 s somatic depolarization of 50–60 mV or by 50–200 somatically triggered action potentials at 50–200 Hz. The consequent depolarization-associated influx of extracellular Ca^{2+} made Ca^{2+} release more likely, presumably by loading intracellular Ca^{2+} stores (Jaffe & Brown, 1994; Yeckel *et al.* 1999; Power & Sah, 2005; Hong & Ross, 2007; Hagenston *et al.* 2008).

Optical data analysis

Episodes of optical data were corrected as follows. Four frames collected before the cell was exposed to excitation radiation were averaged and subtracted from all subsequent frames to correct for dark noise and camera bias. After the experiment, the field of view was moved to a region of the slice devoid of fluorescent processes, and four additional frames were collected. These frames were averaged and subtracted from all frames to correct for tissue autofluorescence. Baseline fluorescence (F) was calculated from the average of at least four frames collected while the cell was exposed to excitation radiation but prior to stimulation. The data were subsequently normalized by calculating $\Delta F/F = |(F(t) - F)|/F$; for brevity we refer to this quantity simply as $\Delta F/F$ or the 'Ca^{2+} signal'. Finally, a 3–5-frame running average of the data was calculated. No frame averaging was carried out on optical data from episodes in which the evaluated Ca^{2+} signal was evoked by brief trains of action potentials. Optical data were not corrected for photobleaching, which typically decreased

bis-fura-2 and fura-2FF fluorescence by less than 3% over 5 s.

Optical data were analysed with either regions of analysis or an analysis line. Regions of analysis were defined using an image of the neuron's baseline fluorescence, and the average signal within each region was calculated for each frame and plotted against time. For the line analysis, a series of connected line segments was drawn along the primary apical dendrite. The Ca^{2+} signal along the line segments – at points separated by the approximate distance between pixels in the image – was determined by interpolating the values at nearby pixels using the ImageLineProfile operation in Igor Pro and plotted as a pseudocolour image, with location along the line represented in the vertical dimension and time represented in the horizontal dimension. Such images are referred to as pseudo-linescans (see Nakamura *et al.* 2000) as they are similar to the images generated by a laser-scanning microscope operating in linescan mode. Ca^{2+} waves appear as diagonal bands in pseudo-linescans.

Analysis of hot and cold spots

Only cells having primary apical dendrites that lay mostly within the plane of focus were chosen to be included in this study. Characterization of hot spots and cold spots was based on variations in the amplitude of Ca^{2+} signals along the length of the dendrite. A section of dendrite was determined to be positive for hot spots and cold spots when changes in the Ca^{2+} signal along its length could be confirmed in all of the optical traces, pseudo-linescans and pseudocolour movies of the Ca^{2+} signal over time. In most instances, confirmation entailed the examination of many Ca^{2+} waves of varying intensity and propagation distance. Potential hot spot–cold spot–hot spot sequences were excluded from the analysis if they were found to be associated with a clear dendritic deformity or a drastic change in dendritic focus.

Immunohistochemistry

Tissue for immunohistochemistry was prepared from 2- to 10-week-old male Sprague–Dawley rats ($n = 6$). Animals were deeply anaesthetized with a ketamine–xylazine–acepromazine mixture and perfused transcardially first with 4% paraformaldehyde–0.05% glutaraldehyde in 0.1 M phosphate buffer (PB; pH = 7.4) and then with aldehyde-free PB. After perfusion, the brains were removed from the skull, sliced coronally or sagittally (60 μm, Leica VT 1000S) and washed in PB overnight. Free-floating sections were washed in 0.05 M Tris-buffered saline (TBS, pH = 7.4) and treated with sodium borohydride/TBS for 10 min to reduce free aldehyde groups. Sections were then washed in TBS and preincubated for 1 h in 10% normal goat serum (NGS; Vector Laboratories) and 0.05% Tween 20 in TBS. Incubation with a polyclonal antibody for the type 1 IP_3R (IP_3R1; Research Genetics, Huntsville, AL, USA) was performed two times overnight at 4°C in 1% NGS and 0.01% Tween 20 in TBS. Control experiments without antibody present did not exhibit labelling (data not shown). Sections were washed in TBS and incubated for 2 h in Alexa 488-conjugated anti-rabbit F(ab′)2 (Invitrogen, Carlsbad, CA, USA), diluted 1 : 500 in TBS. Sections were finally washed repeatedly in TBS, mounted on glass slides, and stored at 4°C. IP_3R1 fluorescence was viewed using an inverted microscope (Zeiss LSM 510; Thornwood, NY, USA) with two-photon excitation from a Ti : Sapphire laser (Chameleon, Coherent Inc., Santa Clara, CA, USA). Stacks of digital micrographs (0.4 μm between images, 0.29 μm pixels) were saved, and CA1 pyramidal neurons were examined for IP_3R1 immunoreactivity. Pyramidal neurons were identified by their pyramid- or ovoid-shaped cell bodies located in stratum pyramidale and by their thick apical dendrites extending into stratum radiatum. Potential clusters of IP_3R1 were initially identified by visual inspection as areas of intense fluorescence that were surrounded by little fluorescence and present in at least three consecutive micrographs. Profiles of fluorescence intensity were then plotted for these sections of dendrite using ImageJ (Wayne Rasband, Bethesda, MD, USA), and linear fits to the intensity were calculated. Clusters were defined as regions where the fluorescence intensity rose above the 95% confidence band of the linear fit for two or more consecutive values. Zeiss LSM Imaging Software was used to measure the distance between cluster edges and to construct 2-D projections from image stacks.

Statistics

As there were no obvious differences in responses across ages, brain regions, or species, data were pooled. Data are presented as mean ± S.E.M. Statistical significance ($P < 0.05$) was tested using Student's unpaired t tests assuming unequal variance (unpaired t test), Student's paired t tests (paired t test), Fisher's Exact tests (Fisher's Exact), or chi-square tests (χ^2), as appropriate.

Results

Ca^{2+} waves triggered by synaptic stimulation exhibit hot spots and cold spots

Simultaneous whole-cell patch-clamp recordings and Ca^{2+} fluorescence imaging were performed on pyramidal neurons from rat hippocampal area CA1 and layer V of the medial prefrontal cortex. Brief trains of synaptic stimulation (30–50 pulses at 100 Hz) evoked propagating rises in $[Ca^{2+}]_i$ that we and others have shown to be

due to the release of Ca^{2+} from intracellular Ca^{2+} stores (Nakamura *et al.* 1999; Kapur *et al.* 2001; Power & Sah, 2002; Larkum *et al.* 2003; Hagenston *et al.* 2008). These Ca^{2+} waves were typically observed in primary apical dendrites ($n = 59$ cells), but were also observed in apical oblique branches ($n = 30$ cells) and occasionally in basal dendrites ($n = 6$ cells). Close examination of $[Ca^{2+}]_i$ rises in contiguous regions of analysis revealed that Ca^{2+} waves often propagated in a non-uniform manner; i.e. in some locations $[Ca^{2+}]_i$ rose higher than in other locations (Fig. 1). Subsequent analysis using higher-resolution pseudo-linescans clearly revealed the non-uniform nature of propagating Ca^{2+} waves. In some dendritic regions, termed 'hot spots', increases in $[Ca^{2+}]_i$ were both larger and more rapid, while in adjacent regions, termed 'cold spots', increases in $[Ca^{2+}]_i$ were smaller and slower. In total, we identified hot spots and cold spots in synaptic stimulation-triggered Ca^{2+} waves from 51 CA1 pyramidal neurons and 6 layer V medial prefrontal cortical pyramidal neurons. We also observed non-uniform Ca^{2+} wave propagation in CA1 pyramidal neurons under conditions in which ionotropic glutamate and GABAergic synaptic transmission were altered pharmacologically. In these experiments, the recording conditions were designed to isolate combined glutamatergic, NMDA receptor-mediated, or AMPA receptor-mediated excitatory postsynaptic currents ($n = 2$, 4 and 1 cells, respectively; see Gipson & Yeckel, 2007). After making our initial observations, we performed experiments under control conditions to specifically examine the likelihood of evoking non-uniform Ca^{2+} waves and found that, in 81% of cells in which Ca^{2+} waves were synaptically elicited, at least one hot spot–cold spot–hot spot sequence could be identified ($n = 35/43$).

Synaptic stimulation-elicited Ca^{2+} waves that propagated through hot spots and cold spots were predominantly observed in primary apical dendrites ($n = 51/59$ cells; Fig. 1*A*), and occasionally in basal dendrites ($n = 4/6$ cells; Fig. 1*B*) and apical oblique dendrites ($n = 2/30$ cells; Fig. 1*C*). It should be noted that it was never an explicit experimental goal or focus of this study to examine internal Ca^{2+} release and Ca^{2+} waves in apical oblique or basal dendrites. Thus, the latter ratios probably represent an underestimate of the proportion of cells for which apical oblique or basal dendritic Ca^{2+} waves might be expected to exhibit non-uniform propagation.

Ca^{2+} waves triggered by focal pharmacological stimulation exhibit hot spots and cold spots

To test whether non-uniform propagation is a general property of Ca^{2+} waves in pyramidal neuron dendrites, and not simply a phenomenon associated with synaptic stimulation, we elicited internal Ca^{2+} release pharmacologically. More specifically, we examined the properties of Ca^{2+} waves triggered by focal pressure application ('puffing') of the group I/II mGluR agonist ACPD (Jaffe & Brown, 1994; Power & Sah, 2007; Hagenston *et al.* 2008) or by focal photolysis ('uncaging') of NPE-caged IP_3 (Stutzmann *et al.* 2003; Hagenston *et al.* 2008). In one series of experiments, we elicited Ca^{2+} waves in individual neurons both with brief trains of synaptic stimulation and by puffing ACPD (400 μM) directly onto their dendrites. As was the case for the cell shown in Fig. 2*A*, waves of internal Ca^{2+} release evoked by synaptic stimulation and ACPD puffing propagated through the same hot spots and cold spots ($n = 4$). Hot spots and cold spots were also observed in neurons where Ca^{2+} waves were triggered with ACPD puffing alone ($n = 3$; data not shown). Further evidence that hot spots and cold spots are a general feature of Ca^{2+} waves, and that their existence is independent of how the waves are elicited, is our finding that Ca^{2+} waves evoked by the focal photolysis of NPE-caged IP_3 also propagated through hot spots and cold spots ($n = 10$; Fig. 2*B*). On the basis of these experimental observations, we conclude that the hot spots and cold spots are an intrinsic feature of propagating Ca^{2+} waves in pyramidal neurons.

The amplitude and rate of rise of Ca^{2+} signals are greater in hot spots than in cold spots

We performed a comprehensive analysis of hot spot–cold spot–hot spot sequences in all of the synaptically stimulated CA1 pyramidal neurons whose Ca^{2+} waves exhibited non-uniform propagation (Fig. 3). We found, as indicated above, that not only was the amplitude of the wave-associated Ca^{2+} signal greater in hot spots than it was in cold spots, but that the rate at which $[Ca^{2+}]_i$ rose was also greater in hot spots. Differences in the kinetics of $[Ca^{2+}]_i$ rises in discrete dendritic domains are evident in the optical traces; these differences are further emphasized in plots of the first time derivative of the Ca^{2+} signal in these domains. For example, in the hot spot–cold spot–hot spot sequence shown in Fig. 3*A*, the maximum amplitude of the first derivative (i.e. the maximum rate at which $[Ca^{2+}]_i$ rose), was nearly three times greater in the two hot spots than it was in the cold spot they flanked. These observations, summarized below, suggest that the mechanisms underlying internal Ca^{2+} release-associated $[Ca^{2+}]_i$ rises in hot spots may be different from those which underlie internal Ca^{2+} release-associated $[Ca^{2+}]_i$ rises observed in cold spots.

To quantify differences in the Ca^{2+} signal between the hot spots and the cold spot in the cell of Fig. 3*A*, we calculated the maximum amplitudes of the Ca^{2+} signals

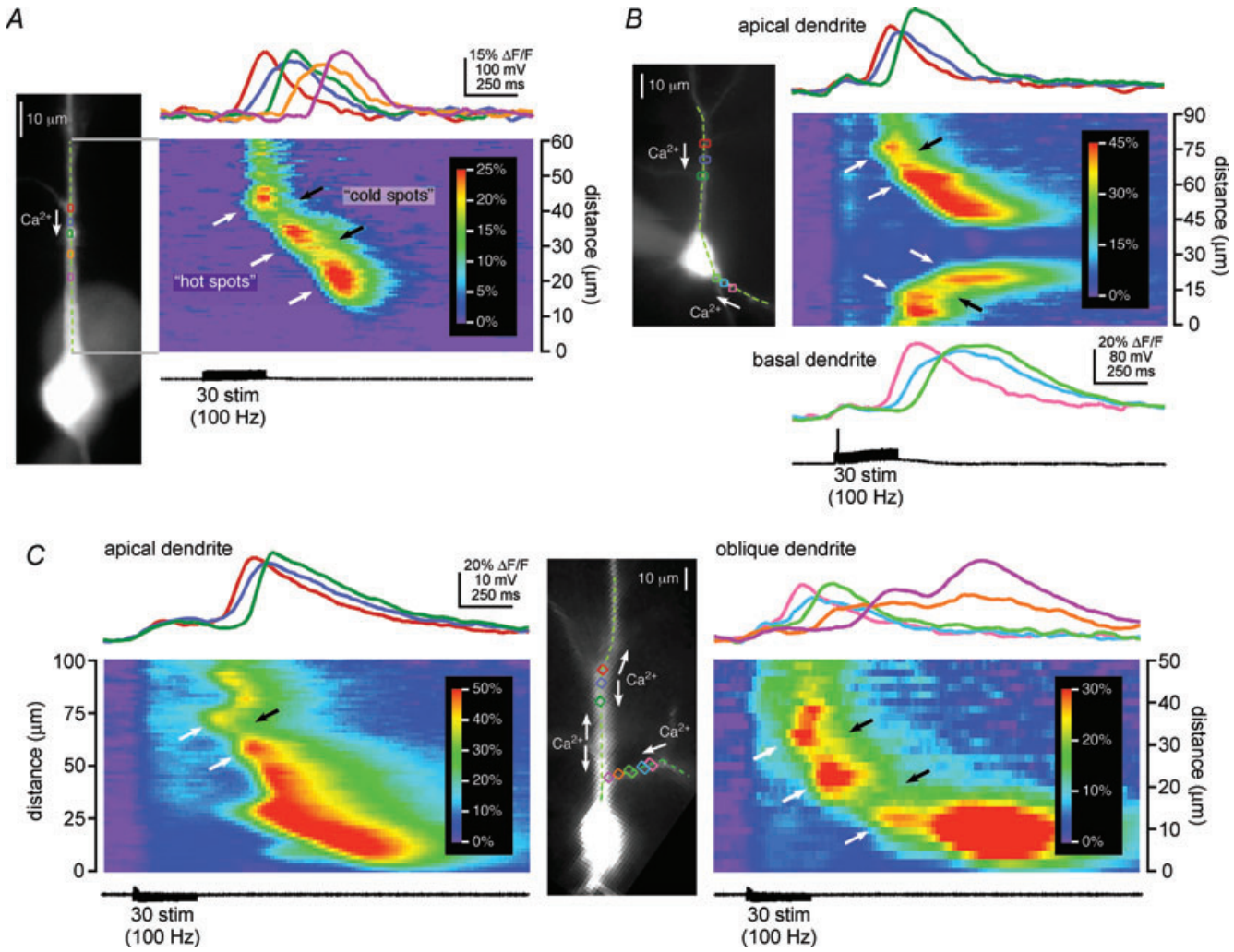

Figure 1. Synaptically triggered Ca^{2+} waves propagate through hot spots and cold spots
A: left, Alexa fluorescence image of a representative CA1 hippocampal pyramidal neuron filled with the Ca^{2+}-sensitive dye fura-2FF. Coloured rectangles define regions of analysis, and the dashed green line identifies the position of the pseudo-linescan; right, Ca^{2+} signals in the analysis regions and along the analysis line during the propagation of a Ca^{2+} wave triggered by synaptic stimulation. The amplitude and rate of rise of the Ca^{2+} wave were high where it initiated at 45 μm in the red region (a hot spot), decreased as the wave propagated through the blue region at 40 μm (a cold spot) and increased again as the wave propagated into the green region at 34 μm (another hot spot). The amplitude and rate of rise subsequently decreased and increased again as the Ca^{2+} wave propagated through an additional cold spot in the orange region at 28 μm into a final hot spot centred on the purple region at 21 μm. Hot spots and cold spots appear in the pseudo-linescan as warmer and cooler colours, and are indicated with white and black arrows, respectively. The stimulation that triggered this Ca^{2+} wave evoked no action potentials (see black voltage trace). *B*: left, image of a layer V medial prefrontal cortical pyramidal neuron filled with the Ca^{2+} indicator bis-fura-2 and showing the position of the analysis line and the analysis regions; right, synaptic stimulation triggered Ca^{2+} waves in both the primary apical dendrite and a basal dendrite of this neuron. The waves in both dendrites propagated from regions of relatively larger amplitude (hot spots; red and pink regions at 75 μm and 15 μm, respectively) through regions of smaller amplitude (cold spots; blue and sky blue regions at 70 μm and 20 μm, respectively) into regions of larger amplitude again (hot spots; green and lime regions at 65 μm and 25 μm, respectively). The rising slope of the Ca^{2+} signal, i.e. its rate of rise, was greater in the hot spots than it was in the cold spots. The stimulation shown here evoked a single action potential and accompanying voltage-dependent rise in $[Ca^{2+}]_i$, evident as a simultaneous and uniform, small increase in the Ca^{2+} signal in all dendritic analysis regions. *C*, synaptic stimulation of this bis-fura-2-filled CA1 pyramidal neuron triggered Ca^{2+} waves in both the primary apical dendrite (left) and in an apical oblique dendrite (right). Left pseudo-linescan and optical traces: the Ca^{2+} wave in the primary apical dendrite initiated in the red region at 78 μm (a hot spot) and propagated through the blue region at 68 μm (a cold spot) before proceeding into the green region at 60 μm (another hot spot). Right pseudo-linescan and optical traces: the Ca^{2+} wave in the apical

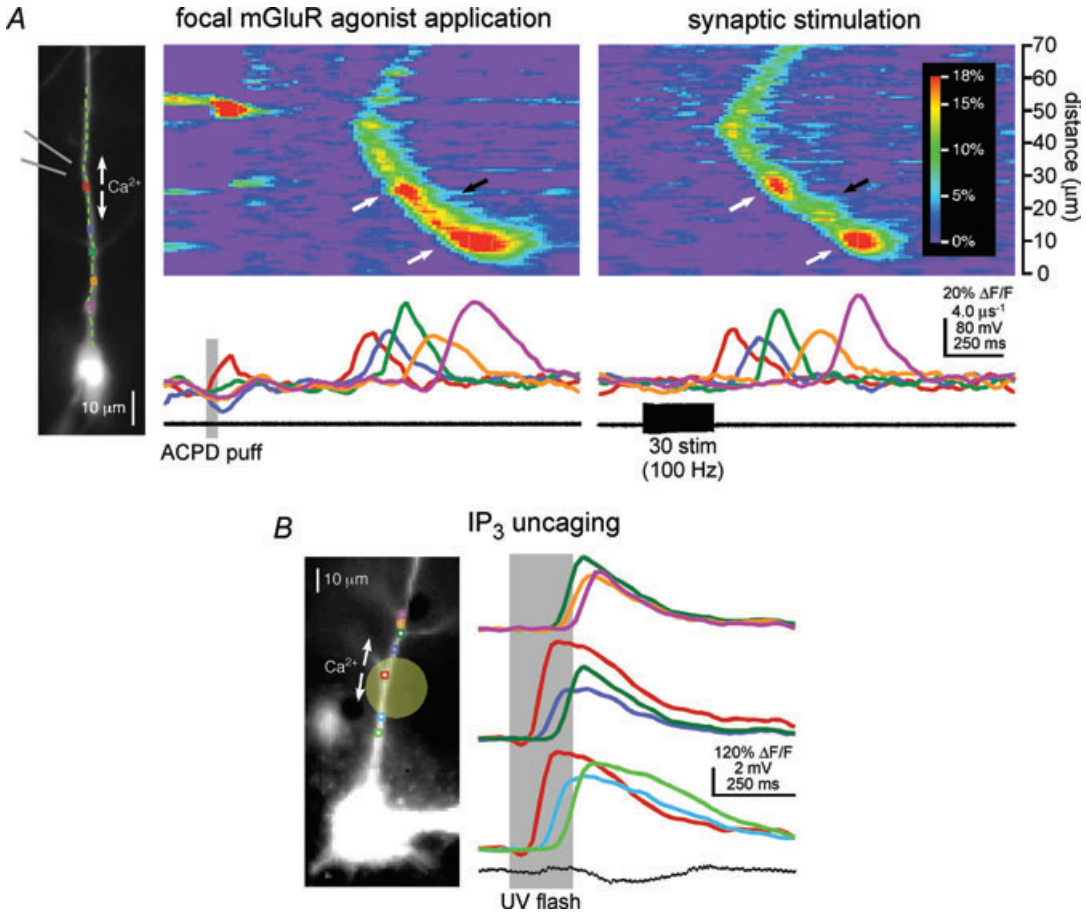

Figure 2. Ca^{2+} waves triggered by focal pharmacological mGluR stimulation and by IP_3 uncaging exhibit hot spots and cold spots

A, Ca^{2+} waves evoked by ACPD puffing and synaptic stimulation propagate through the same hot spots and cold spots. Left, a CA1 pyramidal neuron filled with fura-2FF. The diverging grey lines indicate the approximate position of the puffer pipette adjacent to the primary apical dendrite. Left pseudo-linescan and traces: puffs of ACPD-triggered Ca^{2+} waves that propagated through a hot spot in the green region and a cold spot in the orange region before reaching a final hot spot in the purple region. Right pseudo-linescan and traces: stimulation of synaptic afferents onto this same neuron evoked Ca^{2+} waves that likewise propagated through a hot spot–cold spot–hot spot sequence in the green, orange and purple regions, respectively. *B*, Ca^{2+} waves triggered by focal photolysis of NPE-caged IP_3 propagate through hot spots and cold spots. Left, a CA1 pyramidal neuron filled with NPE-caged IP_3 and the Ca^{2+} indicator dye fluo-4. The pale yellow circle indicates the approximate size and position of the UV uncaging beam. Right, brief flashes of UV light triggered Ca^{2+} waves that initiated in a hot spot at the red region, near the beam's centre, and subsequently propagated bidirectionally. The proximal portion of the Ca^{2+} wave shown here propagated through a cold spot in the sky blue region into a hot spot in the lime region, while the distal portion of this Ca^{2+} wave passed through a cold spot in the blue region and a hot spot in the green region into another cold spot in the orange region and a final hot spot in the purple region.

oblique dendrite initiated in a hot spot centred on the pink region (35 μm), propagated through a cold spot in the sky blue region (30 μm) into a second hot spot in the lime region (25 μm), and then passed through a second cold spot in the orange region (18 μm) before reaching a final hot spot at the dendrite's branch point in the purple region (12 μm). The biphasic Ca^{2+} signal in the purple region represents a summation of $[Ca^{2+}]_i$ increases arising first from the Ca^{2+} wave that originated in the apical oblique dendrite and then from the Ca^{2+} wave that originated in the primary apical dendrite. Both the amplitude of the Ca^{2+} signal and its rising slope were greater in the hot spots than in the cold spots. No action potentials were evoked by this stimulation. This cell was bathed in high divalent (4 mM Ca^{2+} and 5 mM Mg^{2+}) recording ACSF containing 10 μM glycine, 50 μM gabazine, 100 μM D,L-APV, and 1 μM CGP55845.

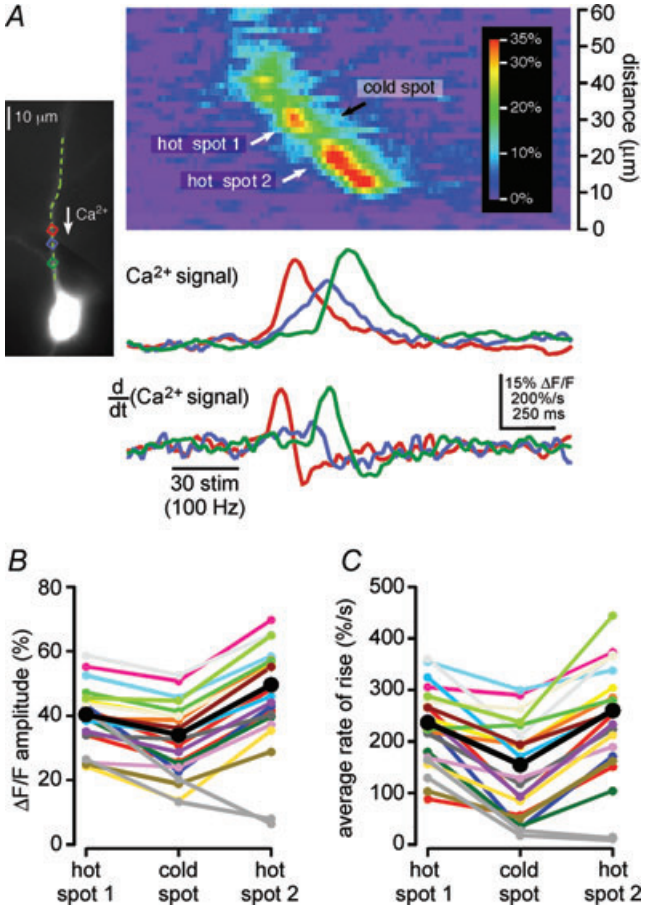

Figure 3. Both the amplitude of internal Ca^{2+} release and rate at which $[Ca^{2+}]_i$ rises during a Ca^{2+} wave are smaller in cold spots than in hot spots: data from a single representative hot spot–cold spot–hot spot sequence
A, left, Ca^{2+} waves triggered by synaptic stimulation in this CA1 pyramidal neuron filled with bis-fura-2 propagated through a hot spot in the red region (hot spot 1), a cold spot in the blue region (cold spot) and another hot spot in the green region (hot spot 2) as they progressed toward the soma. The top set of optical traces shows the amplitude of the Ca^{2+} signal in these three analysis regions as a function of time. The amplitude of the Ca^{2+} wave in both hot spots was greater than it was in the cold spot. The rising slope of the Ca^{2+} signal (i.e. its rate of rise) was also greater in both hot spots than it was in the cold spot. Accordingly, the amplitude of the first derivative of the Ca^{2+} signal, shown in the bottom set of optical traces, was larger in both hot spots than it was in the cold spot. *B*, the maximum amplitude of the fluorescence change in each of hot spot 1, the cold spot and hot spot 2 are plotted for the 21 Ca^{2+} release episodes observed in this cell. The amplitude of the Ca^{2+} signal in hot spot 1 was greater than that in the cold spot for 21 out of 21 Ca^{2+} waves. Similarly, the amplitude of the Ca^{2+} signal in hot spot 2 was greater than that in the cold spot for 19 out of 21 Ca^{2+} waves. Mean values are shown in black. The two Ca^{2+} waves for which the amplitude of fluorescence change in hot spot 2 was less than that in the cold spot represent examples of Ca^{2+} waves that terminated in the cold spot. Their amplitudes, shown in grey, were not included in calculations of mean amplitude. *C*, the plot is of the average rate of rise of the fluorescence change in each of hot spot 1, the cold spot and hot spot 2 for the same 21 Ca^{2+} release episodes depicted in *B*. The average rate of rise in hot spot 1 was greater than that in the cold spot for 20 out of 21 Ca^{2+} waves. Similarly, the average rate of rise in hot spot 2 was greater than that in the cold spot for 19 out of 21 Ca^{2+} waves. Mean values are shown in black. Data corresponding to the two Ca^{2+} waves that failed to propagate through hot spot 2 are again depicted in grey, and were again excluded from calculations of mean rate of rise.

in the hot and cold spots and their average rates of rise between 20% and 80% of these maxima (Fig. 3*B* and *C*). The 21 Ca^{2+} waves observed in this cell exhibited a wide range of amplitudes and rates of rise, such that the amplitudes of the smallest and largest Ca^{2+} waves differed by a factor of three, while the average rates of rise differed by a factor of nearly 4.5. Despite this diversity, the amplitude of the Ca^{2+} signal in this cell's cold spot was always smaller than that in the first hot spot, and smaller than that in the second hot spot for all but 2 of its 21 Ca^{2+} waves (Fig. 3*B*). In the two events for which the Ca^{2+} signal was smaller in the second hot spot, the Ca^{2+} waves terminated at the preceding cold spot. Differences in the average rates of rise of the Ca^{2+} signal in the hot spots and the cold spot were qualitatively similar to differences in the amplitude of the Ca^{2+} signal (Fig. 3*C*). In summary, the average rate of rise of the Ca^{2+} signal in this cell's first hot spot was greater than that in its cold spot in 20 of 21 Ca^{2+} waves, and the average rate of rise of the Ca^{2+} signal in its second hot spot was greater than that in its cold spot in 19 of 21 Ca^{2+} waves (Fig. 3*C*).

The rate of rise of the Ca^{2+} signal decreases more than the amplitude in cold spots

For every synaptically stimulated cell in which we observed non-uniform Ca^{2+} wave propagation, we measured both the amplitude and the average rate of rise of the Ca^{2+} signal in the first hot spot, the cold spot, and the second hot spot for every Ca^{2+} wave that reached all three of these regions (range, 1–28 Ca^{2+} waves per cell; mean, 6 Ca^{2+} waves per cell). We divided the data into two groups based on whether a high-affinity Ca^{2+} indicator dye (bis-fura-2, 100 μM; $n = 35$ hot spot–cold spot–hot spot sequences) or a low-affinity Ca^{2+} indicator dye (fura-2FF, 200 μM; $n = 33$ hot spot–cold spot–hot spot sequences) was used. There were two general differences between these two populations of data unrelated to the hot spot–cold spot–hot spot analyses: the mean amplitudes of $[Ca^{2+}]_i$ rises were significantly greater in cells filled with bis-fura-2 than they were in cells filled with fura-2FF ($P < 0.0001$ for all comparisons, unpaired *t* tests; Fig. 4*A* and *C*), and the average rates at which the Ca^{2+} signals rose were significantly greater for bis-fura-2-filled cells than they were for fura-2FF-filled cells ($P < 0.05$ for all comparisons, unpaired *t* tests; Fig. 4*B* and *D*). More specifically, the mean amplitude of $\Delta F/F$ in leading hot spots (i.e. hot

spot 1 in a hot spot–cold spot–hot spot sequence) was $33 \pm 2\%$ when measured with bis-fura-2, and $20 \pm 1\%$ when measured with fura-2FF. Similarly, the mean rate at which $\Delta F/F$ rose in leading hot spots was $270 \pm 20\%$ s^{-1} when measured with bis-fura-2 and $190 \pm 10\%$ s^{-1} when measured with fura-2FF. Regardless of the Ca^{2+} indicator used, however, both the amplitudes and the rates of rise of Ca^{2+} waves were significantly greater in both leading hot spots and trailing hot spots (i.e. hot spot 2 in a hot spot–cold spot–hot spot sequence) than they were in cold spots ($P < 0.0001$ for all comparisons, paired t tests). For example, the hot spot Ca^{2+} signal for the leading hot spot–cold spot pair was $22 \pm 12\%$ greater than the cold spot Ca^{2+} signal for bis-fura-2-filled cells ($n = 34/35$) and $24 \pm 12\%$ greater for fura-2FF-filled cells ($n = 33/33$). For the trailing cold spot–hot spot pair the hot spot Ca^{2+} signal was $32 \pm 12\%$ greater than the cold spot Ca^{2+} signal for bis-fura-2-filled cells ($n = 35/35$) and $35 \pm 12\%$ greater for fura-2FF-filled cells ($n = 33/33$; Fig. 4*A* and *C*). Similarly, the average rate of $[Ca^{2+}]_i$ rise at the hot spot in the leading hot spot–cold spot pair was $47 \pm 10\%$ faster than that in the cold spot for bis-fura-2-filled cells ($n = 35/35$) and $41 \pm 9\%$ faster for fura-2FF-filled cells ($n = 33/33$); for the trailing cold spot–hot spot pair it was $41 \pm 10\%$ faster for bis-fura-2-filled cells ($n = 34/35$) and $39 \pm 9\%$ faster for fura-2FF-filled cells ($n = 32/33$; Fig. 4*B* and *D*).

Because the percentage differences in the amplitudes of the Ca^{2+} signal and its rates of rise between hot spots and cold spots did not depend on whether a high- or

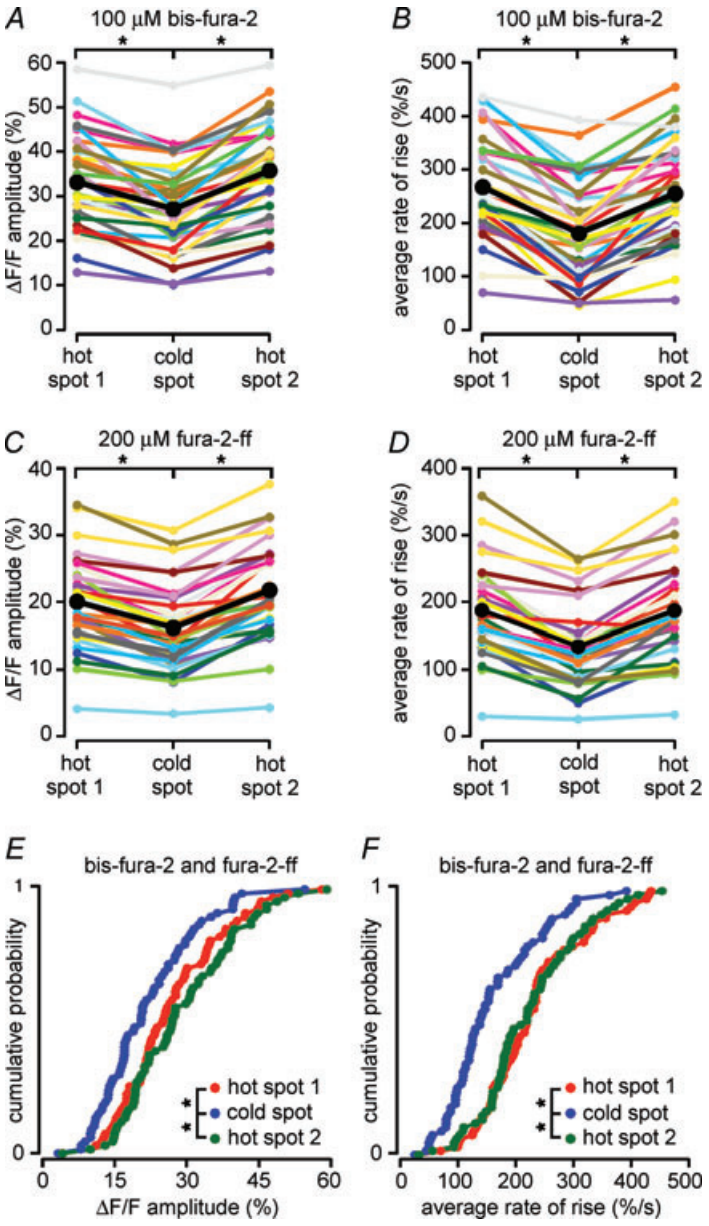

Figure 4. Both the amplitude of internal Ca^{2+} release and rate at which $[Ca^{2+}]_i$ rises during a Ca^{2+} wave are smaller in cold spots than in hot spots: summary data
A–D, differences in the amplitude and kinetics of $[Ca^{2+}]_i$ rises during Ca^{2+} waves were consistent across multiple hot spot–cold spot–hot spot sequences and with both of the relatively higher affinity Ca^{2+} indicator bis-fura-2 (100 μM) and the relatively lower affinity Ca^{2+} indicator fura-2FF (200 μM). Means are shown in black. *A*, plot of the mean amplitudes of Ca^{2+} signals for 35 hot spot–cold spot–hot spot sequences from 29 synaptically stimulated neurons filled with bis-fura-2. Ca^{2+} signals were significantly greater in both hot spots than they were in the cold spot. Data from Ca^{2+} waves that failed to reach the second hot spot were excluded from calculations of the means depicted here and in all subsequent parts of this figure. *B*, average rates of rise of the Ca^{2+} signals for the same 35 hot spot–cold spot–hot spot sequences described in *A*. $[Ca^{2+}]_i$ increased at a significantly faster rate in both hot spots than it did in the cold spot. *C*, plot of the mean amplitudes of Ca^{2+} signals for 33 hot spot–cold spot–hot spot sequences from 23 synaptically stimulated neurons filled with fura-2FF. As was the case for cold spots and hot spots in cells filled with bis-fura-2, the amplitudes of Ca^{2+} signals were significantly greater in both hot spots than they were in the cold spot. *D*, average rates of rise for the same 33 hot spot–cold spot–hot spot sequences described in *C*. The rates of rise of $[Ca^{2+}]_i$ were significantly faster in both hot spots than they were in the cold spot. *E*, cumulative probability plots showing the mean amplitudes of Ca^{2+} signals measured in hot spot 1, the cold spot and hot spot 2 for all 68 hot spot–cold spot–hot spot sequences in all 52 synaptically stimulated neurons filled with either bis-fura-2 or fura-2FF. The amplitudes of internal Ca^{2+} release in the hot spots were significantly greater than those the cold spot. *F*, cumulative probability plots showing the average rates of rise of Ca^{2+} signals for the same 68 hot spot–cold spot–hot spot sequences depicted in *E*. The rates of rise of $[Ca^{2+}]_i$ in the hot spots were significantly faster than those in the cold spot. Statistical significance was determined using Student's paired t tests (*$P < 0.0001$).

low-affinity dye was used (P value ranged from 0.242 to 0.581, unpaired t tests used for all comparisons), we pooled the data sets for all our subsequent analyses. In sum, we found that in 67 of 68 hot spot–cold spot–hot spot sequences from 53 cells, the averaged peak amplitude of the Ca^{2+} wave in both hot spots was greater than the averaged peak amplitude in the cold spot ($24 \pm 6\%$ greater for hot spot 1; $33 \pm 6\%$ greater for hot spot 2; $P < 0.0001$ for both comparisons, paired t tests; Fig. 4*E*). Additionally, we found that the averaged mean rate of rise of the Ca^{2+} signal for all 68 hot spot–cold spot–hot spot sequences was more rapid in both hot spots than it was in the cold spot ($45 \pm 9\%$ faster for hot spot 1; $41 \pm 9\%$ faster for hot spot 2; $P < 0.0001$ for both comparisons, paired t tests; Fig. 4*F*).

As Ca^{2+} waves propagated from the first hot spot into the cold spot, the percentage change in the average rate at which $[Ca^{2+}]_i$ rose was greater than the percentage change in the amplitude of the $[Ca^{2+}]_i$ rise (24% difference in amplitude *vs.* 45% difference in rate of rise; $P < 0.0001$, paired t test). We observed a similar trend in neurons stimulated by puffs of ACPD ($n = 8$ hot spot–cold spot–hot spot sequences, 25% difference in amplitude *vs.* 54% difference in rate of rise; $P = 0.110$, paired t test; data not shown) and to a lesser extent in neurons stimulated with uncaged IP_3 ($n = 12$ hot spot–cold spot–hot spot sequences, 49% difference in amplitude *vs.* 59% difference in rate of rise; $P = 0.091$, paired t test; data not shown). These differences are important because they demonstrate that the Ca^{2+} signal is not simply being attenuated at cold spots, an observation one might make if the cold spot were an artifact produced by a quirk in our optics or by an error in our data analysis. These findings strengthen our suggestion that the mechanisms underlying internal Ca^{2+} release-associated $[Ca^{2+}]_i$ rises in hot spots and cold spots are different.

VGCC-dependent Ca^{2+} signals do not have hot spots and cold spots

$[Ca^{2+}]_i$ rises in neurons are traditionally thought to result from the influx of extracellular Ca^{2+} through VGCCs and ligand-gated Ca^{2+} channels. To test whether the Ca^{2+} signals mediated by these ion channels might exhibit hot spots and cold spots, we compared the VGCC-mediated $[Ca^{2+}]_i$ rises elicited by back-propagating actions potentials (1–5 action potentials at 100–200 Hz) with the Ca^{2+} wave-associated $[Ca^{2+}]_i$ rises triggered by synaptic stimulation. We found that VGCC-mediated rises in $[Ca^{2+}]_i$ occur relatively simultaneously along the apical dendrites of CA1 and layer V medial prefrontal cortical pyramidal neurons, and that they do not exhibit hot and cold spots. For example, in the CA1 pyramidal neuron shown in Fig. 5, action potentials evoked by somatic depolarization generated simultaneous and uniform rises in $[Ca^{2+}]_i$ along the proximal apical dendrite. By contrast, synaptic stimulation-triggered Ca^{2+} waves in this same neuron propagated through two hot spots and a cold spot ($n = 15$ waves). For each of the 10 trains of action potentials evoked in this cell, the amplitude of the VGCC-mediated Ca^{2+} signal was nearly identical in all of the hot and cold spots (Fig. 5*A* and *C*). We made similar measurements for a total of 16 hot spot–cold spot–hot spot sequences ($n = 14$ cells; Fig. 5*C*). In each case, we found that the amplitudes of Ca^{2+} waves in both hot spots were significantly greater than those in the cold spot ($30 \pm 21\%$ greater for hot spot 1; $52 \pm 19\%$ greater for hot spot 2; $P < 0.0001$ for both comparisons, paired t tests). The amplitudes of Ca^{2+} signals evoked by action potentials in the same hot and cold spots did not, however, exhibit any significant differences ($3 \pm 24\%$ greater for hot spot 1; $P = 0.136$, paired t test; $0 \pm 25\%$ greater for hot spot 2; $P = 0.907$, paired t test). These data demonstrate that variations in the amplitudes of Ca^{2+} wave-associated Ca^{2+} signals along dendrites do not exist for Ca^{2+} signals produced by influx through VGCCs. These data also show that the variations in Ca^{2+} signals observed during Ca^{2+} waves are not due to location-dependent variations in our ability to detect Ca^{2+} signals, nor do they result from some error in the data analysis.

Ca^{2+} waves initiate in hot spots

Our observation that both the amplitude of a Ca^{2+} wave and its rate of rise are greater in hot spots than in cold spots suggests that intracellular Ca^{2+} stores are more capable of releasing Ca^{2+} in a regenerative fashion in hot spots than they are in cold spots. This conclusion is supported by an additional observation: both leading and trailing hot spots are capable of initiating Ca^{2+} waves (see Figs 1, 6 and 9*A*). For example, in the CA1 pyramidal neuron shown in Fig. 6, Ca^{2+} waves sometimes propagated through a series of hot spots and cold spots, and other times initiated where the hot spots had been or would have been. In particular, in the most robust internal Ca^{2+} release events in this cell, Ca^{2+} waves exhibited three clear initiation sites (50 μm, 33 μm and 18 μm from the soma; upper-left pseudo-linescan). Less robust Ca^{2+} waves typically initiated either at only the middle of these three sites (33 μm; e.g. upper-right and lower-left pseudo-linescans) or the most distal of these sites (50 μm; e.g. bottom-centre and bottom-right pseudo-linescans). For some of these Ca^{2+} waves, the portion of dendrite centred on 18 μm experienced a rise in $[Ca^{2+}]_i$ prior to arrival of the more distally initiated Ca^{2+} wave (upper-right pseudo-linescan; see steepening of the wave front that appears as a slight leftward bulge). In other recordings of these release events, however, Ca^{2+} waves propagated smoothly through the

portion of dendrite 18 μm from the soma (bottom-left and bottom-right pseudo-linescan). In all of these less robust events, however, the amplitude and rate of rise of the Ca^{2+} signal at 18 μm were greater than those in adjacent portions of the dendrite. Therefore, this location, which for some Ca^{2+} release events could be characterized as an initiation site, might for other events be best called a 'premature Ca^{2+} release site' or a 'late initiation site,' or for still other events may be simply described as a hot spot. Like the portion of dendrite centred on 18 μm, the section of dendrite at 33 μm, when it was not the site of Ca^{2+} wave initiation, could also be described either as a premature Ca^{2+} release site (bottom-right pseudo-linescan) or as a hot spot (bottom-centre pseudo-linescan). Thus, of the three Ca^{2+} wave initiation sites documented for this cell, two were also observed to be hot spots.

An examination of all hot spots and initiation sites identified in the synaptically stimulated neurons of this study revealed that 56% of all initiation sites were also hot spots ($n = 74/131$ initiation sites) and that 57% of all hot spots were also initiation sites ($n = 74/129$ hot spots). Furthermore, 89% of all leading hot spots and 33%

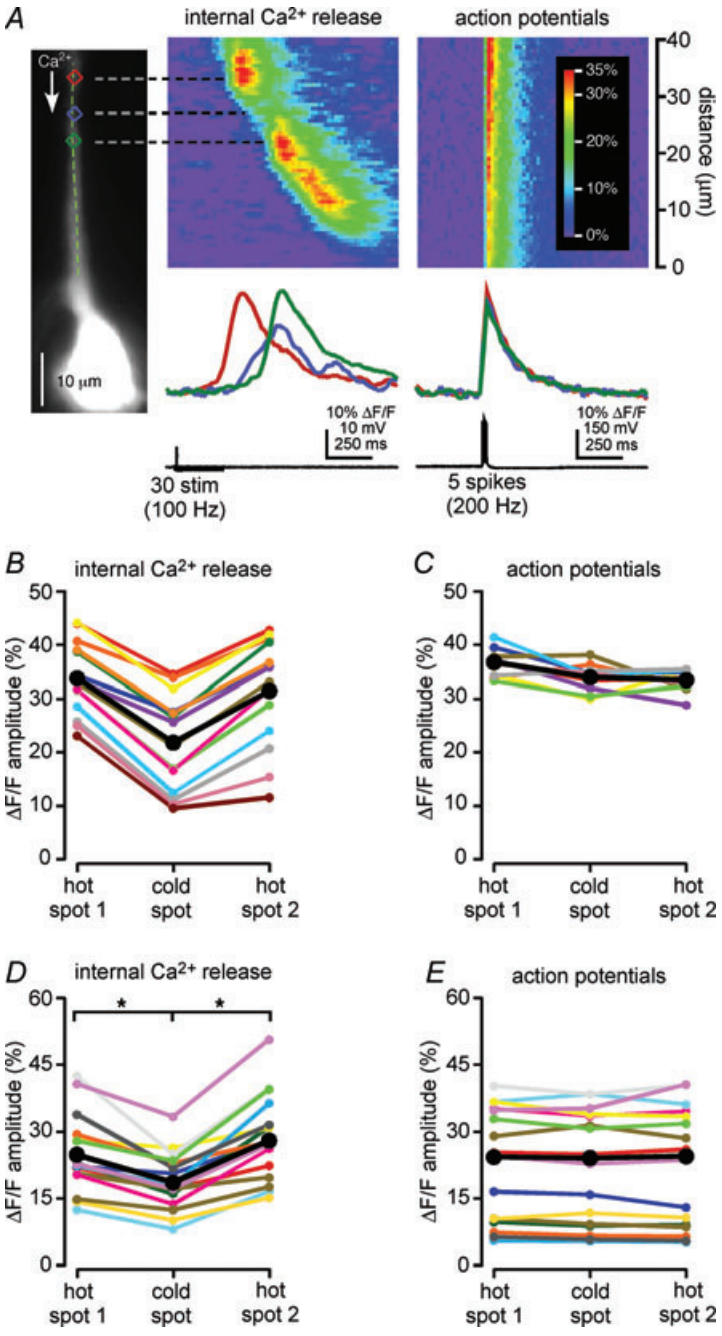

Figure 5. Dendritic Ca^{2+} signals evoked by action potentials do not exhibit hot spots and cold spots
A, left, a CA1 pyramidal neuron filled with bis-fura-2. Left pseudo-linescan and traces, synaptic stimulation triggered Ca^{2+} waves that varied in amplitude as they traversed the primary apical dendrite. The amplitude of the Ca^{2+} signal was largest in the two hot spots centred on the red and green analysis regions and smallest in the cold spot in the blue analysis regions between them. Right pseudo-linescan and traces, large, brief current injections were used to trigger five action potentials in the same cell. The amplitude of the Ca^{2+} signal produced by the action potentials was nearly uniform along the same length of the primary apical dendrite and in each of the red, blue and green analysis regions. The data depicted here represent an average of ten episodes. *B*, the amplitudes of Ca^{2+} signals were greater in the hot spots than in the cold spot in all 15 Ca^{2+} waves observed in this cell. Mean values are shown in black. *C*, in contrast, each of ten bursts of action potentials produced Ca^{2+} signals of nearly identical amplitude in all of the first hot spot, the cold spot and the second hot spot. Mean values are shown in black. *D*, plot of the mean amplitudes of Ca^{2+} signals evoked by synaptic stimulation for 16 hot spot–cold spot–hot spot sequences from 14 neurons. The amplitudes of Ca^{2+} signals were significantly greater in the hot spots than in the cold spot. Means are shown in black. *E*, plot of the mean amplitudes of Ca^{2+} signals triggered by brief trains of action potentials (1–5 spikes at 100–200 Hz) for the same 16 hot spot–cold spot–hot spot sequences depicted in *D*. Hot spots and cold spots exhibited nearly identical $[Ca^{2+}]_i$ rises during trains of action potentials. Means are shown in black. Statistical significance was determined using Student's paired *t* tests (*$P < 0.0001$).

of all trailing hot spots initiated Ca^{2+} waves ($n = 50/56$ leading hot spots; $n = 24/73$ trailing hot spots). These observations emphasize the functional similarity between initiation sites and hot spots, and suggest again that Ca^{2+} wave-associated $[Ca^{2+}]_i$ rises in hot spots are generated by mechanisms distinct from the $[Ca^{2+}]_i$ rises observed in adjacent dendritic regions. More specifically, our data are consistent with the hypothesis that Ca^{2+} wave-associated $[Ca^{2+}]_i$ rises in hot spots are mediated by the intracellular release of Ca^{2+}, while Ca^{2+} wave-associated $[Ca^{2+}]_i$ rises in cold spots arise due to the diffusive spread of Ca^{2+} away from and between release sites.

Most hot spots are located at branch points

It has been shown previously that synaptically stimulated Ca^{2+} waves initiate at branch points (Nakamura *et al.* 2002). We observed that both leading and trailing hot spots can behave as Ca^{2+} wave initiation sites (Figs 1*A–C*, 6 and 9*A*). We therefore examined the propensity for hot spots to be located at dendritic branch points or at locations where the primary apical dendrite divides to form two dendrites with approximately the same diameter ('dendritic bifurcations'). In all, 84% of hot spots ($n = 100/119$) and 6% of cold spots ($n = 4/68$) were located at identified dendritic branch points or bifurcations (Fig. 7*A* and *B*). Likewise, 70% of identified dendritic branch points ($n = 88/126$) and 92% of identified dendritic bifurcations ($n = 12/13$) through which Ca^{2+} waves were observed to propagate were hot spots. In contrast, only 3% of identified dendritic branch points and bifurcations were cold spots ($n = 4/139$; Fig. 7*B*). Significantly more hot spots than cold spots were located at branch points ($n = 100/119$ hot spots *vs.* $n = 4/68$ cold spots, $P < 0.0001$, Fisher's Exact), and significantly more branch points and bifurcations were

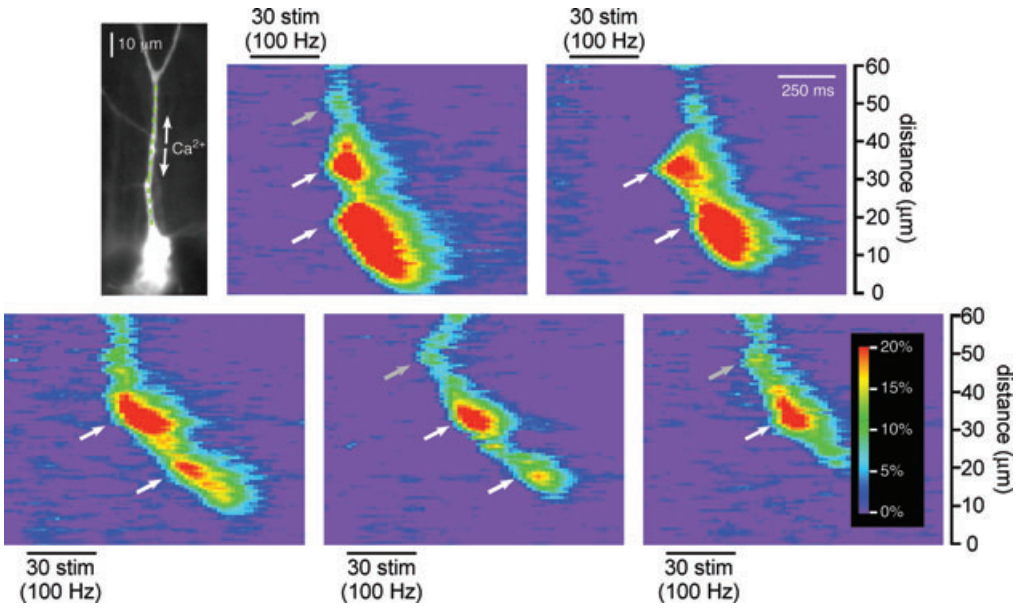

Figure 6. Ca^{2+} waves initiate in hot spots
Left, a CA1 pyramidal neuron filled with fura-2FF. Right, synaptic stimulation triggered Ca^{2+} waves of varying intensity and propagation extent in this cell, five of which are shown here. In the most robust Ca^{2+} wave, depicted in the upper left pseudo-linescan, there appear to be three independent initiation sites – at 55 μm, 33 μm and 18 μm – that released Ca^{2+} almost simultaneously. These locations are indicated with arrows. In a slightly less robust Ca^{2+} wave, depicted in the upper right pseudo-linescan, a wave of internal Ca^{2+} release initiated at 33 μm and propagated toward the soma, where it encountered a section of dendrite, centred on 18 μm, where Ca^{2+} had already been released. The location of this early release site is the same as that of the most proximal initiation site in the upper left pseudo-linescan and that of the most proximal hot spot in the bottom left and bottom centre pseudo-linescans. Another Ca^{2+} wave of moderate intensity, depicted in the bottom left pseudo-linescan, initiated at 33 μm and then propagated smoothly through a region of relatively smaller amplitude (a cold spot) before reaching a region of relatively larger amplitude (a hot spot) at 18 μm. The Ca^{2+} wave depicted in the bottom centre pseudo-linescan did not initiate at 33 μm, but rather at 55 μm, and then propagated into a region of relatively larger amplitude at 33 μm (a hot spot), through a cold spot and finally into the hot spot at 18 μm. Thus, the 33 μm and 18 μm initiation sites in the most robust Ca^{2+} wave observed in this cell also behaved as hot spots with an interposed cold spot in less robust Ca^{2+} waves. The least robust Ca^{2+} waves in this cell, like that shown in the bottom right pseudo-linescan, not only failed to propagate into the second hot spot at 18 μm, but also failed in the cold spot immediately preceding it.

hot spots than were cold spots ($n = 100/139$ branch points *vs.* 4/139 branch points, $P < 0.0001$, Fisher's Exact). In summary, most hot spots, but only very few cold spots, are located at dendritic branch points. These findings suggest that dendritic branch points may be better endowed for the generation of IP_3R-mediated rises in $[Ca^{2+}]_i$ than the portions of dendrite between them.

Type 1 IP_3 receptors form clusters at branch points and along the length of primary apical dendrites

$[Ca^{2+}]_i$ rises in the dendritic domains that we characterized as hot spots exhibited both larger amplitudes and faster kinetics than those in adjacent regions of dendrite. Moreover, these hot spots, which can also initiate Ca^{2+} waves, tend to be located at dendritic branch points. These findings suggest not only that dendritic domains in which hot spots reside may have an enhanced capacity for regenerative internal Ca^{2+} release, but also that they may be intrinsically enriched for the cellular and molecular machinery that enable intracellular Ca^{2+} release. Perhaps the most important component of this machinery in pyramidal neurons is the IP_3R itself. In order to determine whether the distribution of IP_3Rs along dendrites might provide a biochemical basis for the existence and distribution of hot spots, we performed an immunohistochemical analysis of type 1 IP_3Rs (IP_3R1) in CA1 pyramidal neurons ($n = 6$ rats). We focused on IP_3R1 because it is the most prevalent IP_3R subtype in the hippocampus and neocortex (Sharp *et al.* 1999;

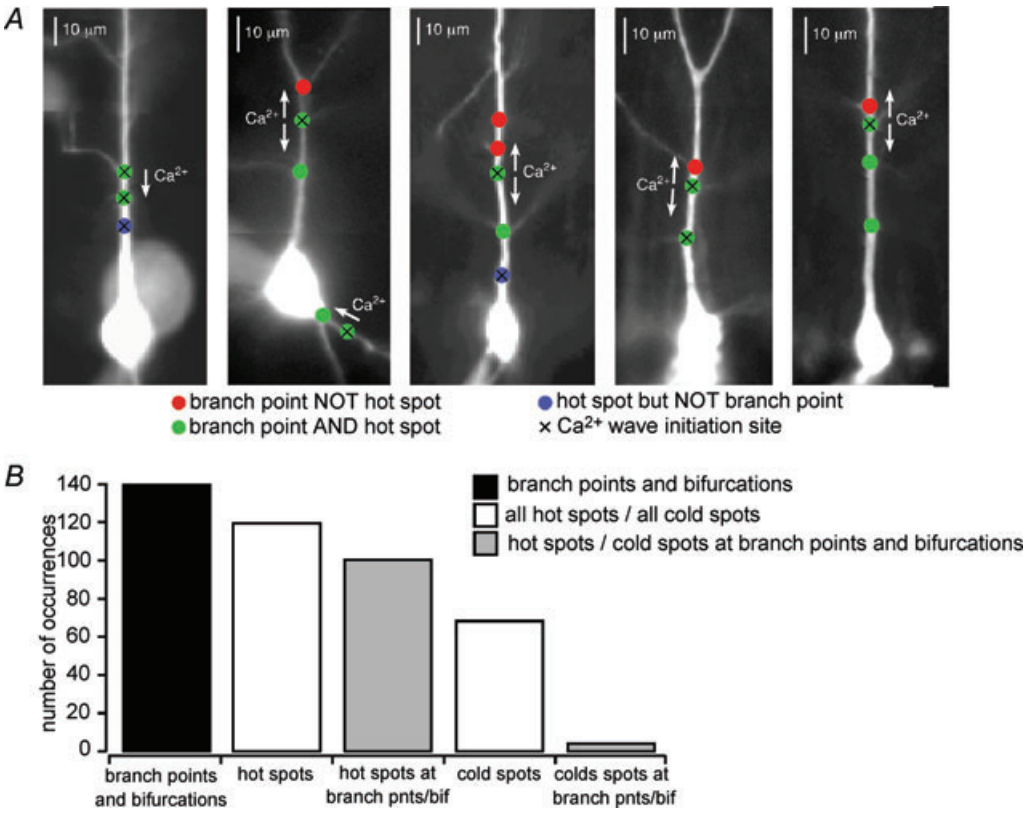

Figure 7. Most hot spots are located at dendritic branch points
A, coloured circles indicate the locations of hot spots and branch points through which synaptic stimulation-evoked Ca^{2+} waves propagated in five representative cells. Red circles denote the locations of identified branch points that lay in the paths of observed Ca^{2+} waves. Green circles denote the locations of branch points that were identified to be hot spots. Blue circles denote the locations of hot spots where no oblique branching was visualized. Black Xs denote the locations of initiation sites. Pseudo-linescans and optical traces for the cells shown here, from left to right, are depicted in Figs 1*A* and *B*, 2*A*, 6 and 9*A*, respectively. *B,* plot of the total number of identified dendritic branch points and bifurcations in the paths of Ca^{2+} waves in 49 synaptically stimulated cells, the total number of identified hot spots in this same population of cells and the total number of hot spots located at branch points or bifurcations, as well as the total number of cold spots in this same population of cells and the total number of cold spots located at branch points. Most identified branch points and bifurcations in the paths of Ca^{2+} waves were also hot spots ($n = 100/139$ branch points, 72%) and most hot spots were located at identified branch points or bifurcations ($n = 100/119$ hot spots; 84%), while only very few branch points were also cold spots ($n = 4/139$ branch points, 3%) and very few cold spots were located at identified branch points ($n = 4/68$ cold spots, 6%).

Hertle & Yeckel, 2007). Consistent with our previous findings showing IP_3R1 clustering in the dendritic branch points of CA1 pyramidal neurons (Hertle & Yeckel, 2007), and with reports of IP_3R clustering in other cell types (Oberdorf *et al.* 1997; Boulware & Marchant, 2005; Tateishi *et al.* 2005; Shuai *et al.* 2006), we observed a non-uniform distribution of IP_3R1 immunofluorescence along pyramidal neuron dendrites (Fig. 8*A* and *B*). We quantified these data by measuring the intensity of IP_3R1 immunofluorescence along pyramidal neuron primary apical dendrites, plotting the results, and then calculating linear fits to each data set (see Fig. 8*C*). Clusters of IP_3R1 immunoreactivity were subsequently defined as dendritic domains where the IP_3R1 immunofluorescence intensity rose above the upper 95% confidence band of the linear fit. The staining technique employed made it difficult to compare the locations of these IP_3R1 clusters to the locations of dendritic branch points. We therefore sought, as an alternative, to compare the distances between adjacent IP_3R1 clusters in CA1 pyramidal neurons with the distances between adjacent hot spots in this same cell type (Fig. 8*C*). Our measurements reveal that the distributions

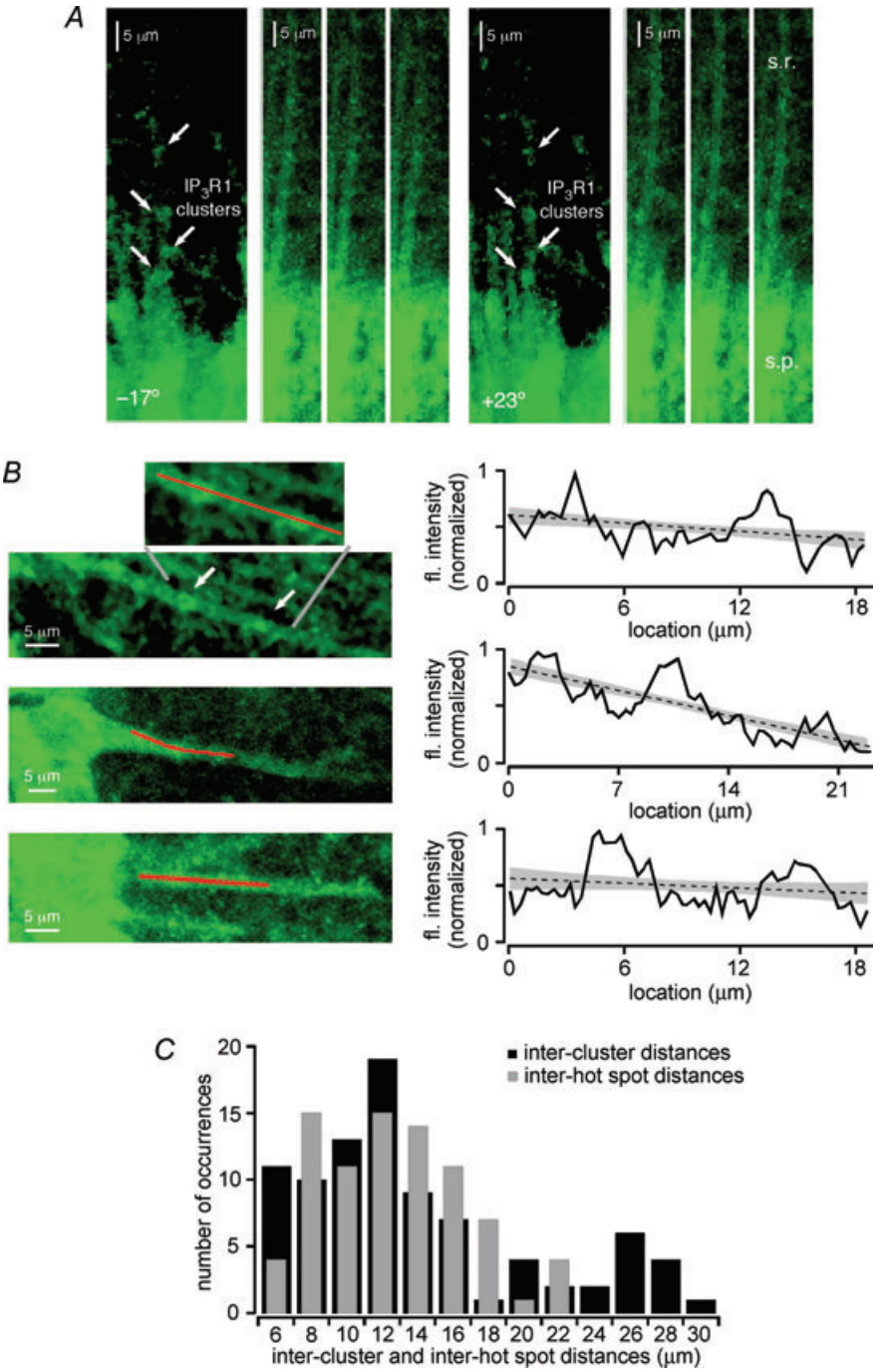

Figure 8. IP_3R1s are distributed in clusters along the primary apical dendrites of CA1 hippocampal pyramidal neurons
A and *B*, the distribution of IP_3R1s in CA1 pyramidal neurons was examined using immunohistochemistry. *A*, digital confocal images of IP_3R1 immunofluorescence were recorded at 0.4 μm intervals from six rats. Projections at −17 deg and +23 deg were made from image stacks depicting IP_3R1 immunoreactivity along a single apical dendrite in stratum radiatum of hippocampal area CA1. Four clusters of immunofluorescence, indicated with arrows, are evident along this dendrite. Individual images in different focal planes of the same primary apical dendrite show the same four clusters of immunofluorescence along its length. *B*, left, images of three different primary apical dendrites exhibiting clusters of IP_3R1 immunoreactivity. Red lines indicate sections of dendrite evaluated for immunofluorescence intensity. Right, plots of fluorescence intensity along the analysis lines of the three primary apical dendrites depicted at left. Linear fits to the fluorescence intensity data are indicated with dashed lines, while grey shading denotes 95% confidence bands. Fluorescence intensity rises above the upper 95% confidence band at two or three locations along each section of dendrite. These locations coincide with visible clusters of IP_3R1 immunoreactivity in the images at left. *C*, plot of the distribution of distances between the edges of 89 pairs of adjacent IP_3R1 clusters from 36 apical dendrites (black bars) and the distribution of distances between the centres of 82 pairs of adjacent hot spots from 62 cells (grey bars). There is no significant difference between the two distributions ($P = 0.218$, unpaired t test).

of inter-cluster and inter-hot spot distances are statistically indistinguishable (IP_3R1 clusters, $13.7 \pm 0.7\,\mu$m, $n = 89$ cluster pairs; hot spots, $12.7 \pm 0.4\,\mu$m, $n = 82$ hot spot pairs; $P = 0.218$, unpaired t test). These and our previous immunohistochemical findings (Hertle & Yeckel, 2007) strongly support the likelihood that IP_3R clustering, particularly at branch points, underlies the non-uniform initiation and propagation of Ca^{2+} waves in pyramidal neuron dendrites.

Ca^{2+} waves terminate in cold spots

The characteristics of propagating Ca^{2+} waves can be highly diverse. Some Ca^{2+} waves may propagate continuously along their entire extent (data not shown), while others propagate continuously but for their passage through a single cold spot (see Figs 3 and 5). Some Ca^{2+} waves might propagate through multiple hot spots and cold spots in a saltatory fashion (see Figs 1*A* and 9) while still other waves may hardly propagate at all, but instead appear as distinct, compartmentalized puffs of Ca^{2+} (data not shown). A similar diversity in the characteristics of propagating Ca^{2+} waves has been observed in many non-neuronal cell types, including HeLa cells (Bootman *et al.* 1997), *Xenopus* (Callamaras *et al.* 1998; Callamaras & Parker, 1998), cardiac myocytes (Cheng *et al.* 1993), and astrocytes (Yagodin *et al.* 1994). In these cells, Ca^{2+} wave propagation tends to be continuous when very high agonist concentrations are employed or when $[IP_3]_i$ is far above threshold. When the concentration of agonist or $[IP_3]_i$ lies just above the threshold for regenerative Ca^{2+}-induced Ca^{2+} release, however, Ca^{2+} wave propagation appears saltatory. At still lower agonist concentrations of $[IP_3]_i$, small amounts of Ca^{2+} are released in 'puffs' or 'sparks' at those locations where the amplitude of the Ca^{2+} wave had been the largest, and no propagation is observed. These observations suggest that the non-uniform propagation of Ca^{2+} waves (i.e. through hot spots and cold spots) depends on the release of large boluses of Ca^{2+} from hot spots. These findings also suggest that Ca^{2+} waves are most likely to fail between hot spots when the $[Ca^{2+}]_i$ liberated by one hot spot is insufficiently large to cross the diffusion barrier posed by its adjoining cold spots. Our results are consistent with these ideas. In particular, we found that when Ca^{2+} waves failed to propagate through a complete series of hot spots and cold spots, they did not fail at random locations. Rather, Ca^{2+} waves tended to terminate in cold spots (Figs 6 and 9). Moreover, we found that both the amplitude and the rate of rise of $[Ca^{2+}]_i$ in the first hot spot were significantly smaller for Ca^{2+} waves that failed in the cold spot than they were for Ca^{2+} waves that propagated through the cold spot and into the second hot spot.

An example of cold spot Ca^{2+} wave failure can be seen in Fig. 9. The most robust Ca^{2+} waves in the cell of this figure propagated through three hot spots and two intervening cold spots before terminating (left pseudo-linescan). Other Ca^{2+} waves propagated through the first hot spot and cold spot and into the second hot spot, but failed to propagate beyond the second cold spot (middle pseudo-linescan). Still other Ca^{2+} waves propagated out of the first hot spot, but then failed to propagate beyond the first cold spot (right pseudo-linescan). Of the ten Ca^{2+} waves examined in this cell, six terminated in the first cold spot, two terminated in the second cold spot and two terminated after the third hot spot (Fig. 9*B*). In other words, if the section of dendrite immediately proximal to the third hot spot were to be considered a cold spot, then it may be said that all of the Ca^{2+} waves examined in this cell terminated in cold spots.

We examined 93 Ca^{2+} waves propagating through 42 hot spot–cold spot–hot spot sequences in 35 neurons. A Ca^{2+} wave was judged to have terminated in the cold spot when there was a 50% or greater reduction in the amplitude of the Ca^{2+} signal and/or its average rate of rise between the cold spot and the second hot spot. In all other cases, the Ca^{2+} wave was considered to have terminated in or after the second hot spot. Our analysis shows that 86% of Ca^{2+} waves terminated in the cold spot ($n = 80/93$), a significantly greater proportion than that of waves which terminated in or after the second hot spot ($n = 13/93$; $P < 0.0001$, $\chi^2 = 48.3$). We also compared the characteristics of Ca^{2+} waves that successfully propagated through the cold spot with those of Ca^{2+} waves that failed in the cold spot (Fig. 9*E* and *F*). Both the amplitude and the rate of rise of Ca^{2+} signals in leading hot spots were consistently greater for Ca^{2+} waves that propagated through the cold spot than they were for Ca^{2+} waves that failed in the cold spot (amplitude, $n = 29/42$, $10 \pm 9\%$ greater, $P < 0.001$, paired t test; rate of rise, $n = 37/42$, $26 \pm 8\%$ greater, $P < 0.0001$, paired t test). These data suggest that the regions of dendrite we have characterized as cold spots may serve as a barrier to Ca^{2+} wave propagation when the conditions and/or stimuli that trigger internal Ca^{2+} release are sub-optimal.

Discussion

We studied the basic properties of intracellular Ca^{2+} waves in the dendrites of CA1 and layer V medial prefrontal cortical pyramidal neurons, and found that these Ca^{2+} waves propagate in a non-uniform manner. In some locations, which are frequently associated with dendritic branch points, the amplitude and rate of rise of the Ca^{2+} signals are consistently large. In other locations, the amplitude and rate of rise of the Ca^{2+} signals are consistently smaller. These sites, which we call 'hot spots'

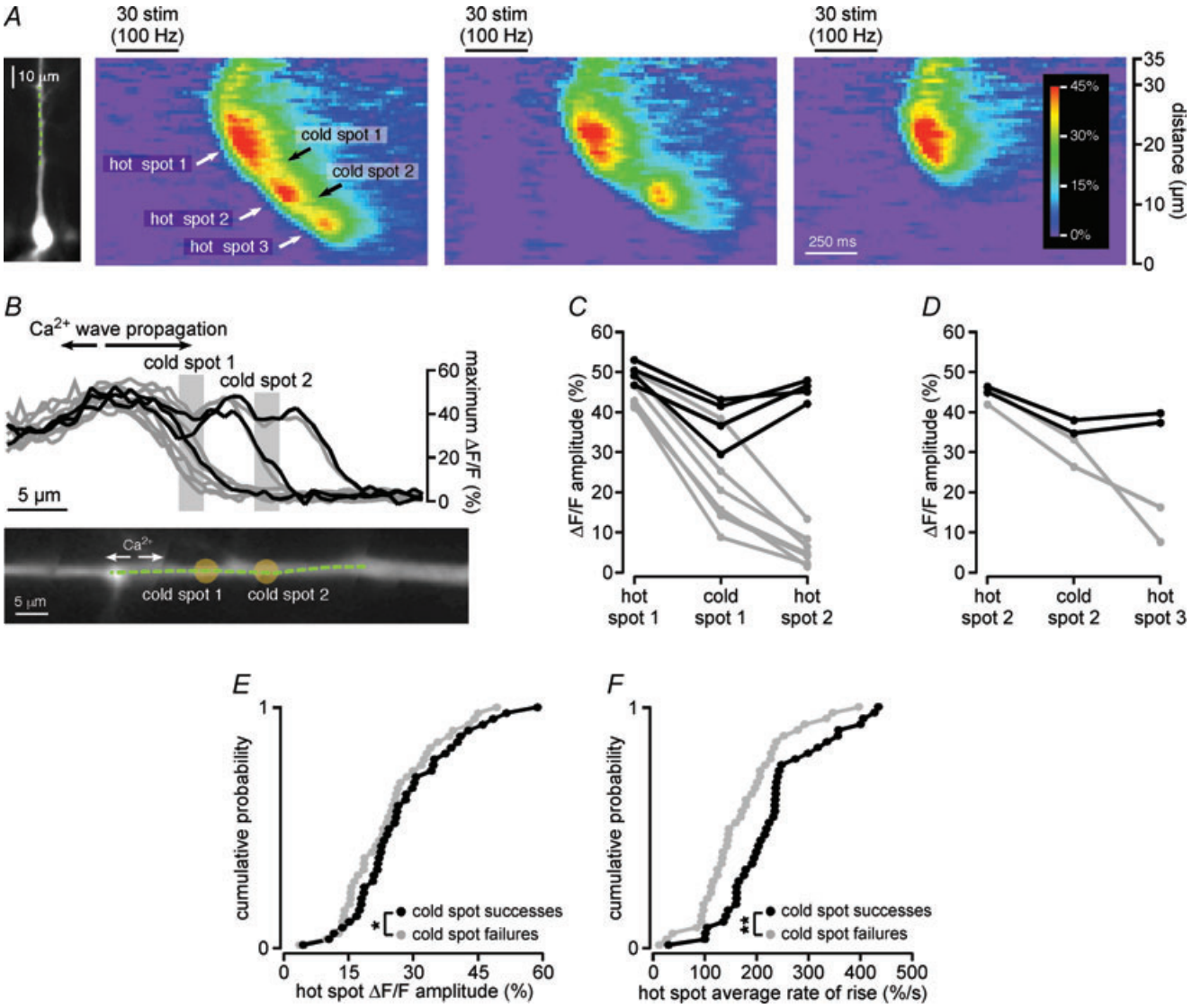

Figure 9. Ca^{2+} waves terminate in cold spots

A, left, a CA1 pyramidal neuron filled with bis-fura-2. Right, synaptic stimulation triggered Ca^{2+} waves of variable extent in this cell. The most robust Ca^{2+} waves, like that depicted in the left pseudo-linescan, propagated through three hot spots and two cold spots. Less robust Ca^{2+} waves, like that depicted in the centre pseudo-linescan, failed to propagate beyond the second cold spot into the third hot spot. The weakest Ca^{2+} waves, like that shown in the right pseudo-linescan, terminated in the first cold spot prior to reaching the second hot spot. *B*, top, plot of the maximum amplitude of the Ca^{2+} signal *versus* location on the analysis line for multiple Ca^{2+} waves observed in the cell shown in *A*. Cold spots are evident in the plot as regions of consistently smaller amplitude Ca^{2+} signal separated by regions of relatively larger amplitude Ca^{2+} signal (hot spots). Cold spot locations are indicated with pale grey bars. The plot shows that two Ca^{2+} waves propagated through all three hot spots, and then terminated after the third hot spot. Two Ca^{2+} waves propagated through the first and second hot spots, but failed in the second cold spot, and six Ca^{2+} waves propagated through the first hot spot, but subsequently failed in the first cold spot. The three black traces correspond to the Ca^{2+} waves depicted in *A*. Bottom, an enlarged image of the dendrite along which internal Ca^{2+} release amplitude was evaluated. The dashed green line indicates the position of the analysis line. Pale yellow circles indicate the positions of cold spots. *C*, plot of the maximum amplitudes of Ca^{2+} signals in the first hot spot, the first cold spot and the second hot spot for ten Ca^{2+} waves evoked in the cell depicted in *A* and *B*. Shown in black are the amplitudes of Ca^{2+} signals for Ca^{2+} waves that propagated through the second hot spot, and in grey the amplitudes of Ca^{2+} signals that terminated in the first cold spot. *D*, the maximum amplitudes of Ca^{2+} signals in the second hot spot, the second cold spot and the third hot spot for the four Ca^{2+} waves that propagated through the second hot spot in the cell depicted in *A*, *B* and *C*. Shown in black are the amplitudes of Ca^{2+} signals for two Ca^{2+} waves that propagated through the third hot spot, and in grey the amplitudes of Ca^{2+} signals that failed in the second cold spot. *E*, cumulative probability plots showing the

and 'cold spots', respectively, appear to differ in terms of their capability to support regenerative internal Ca^{2+} release. More specifically, we observed that Ca^{2+} wave initiation tends to occur in dendritic domains that are characterized as hot spots and that Ca^{2+} wave failure tends to occur in domains that are characterized as cold spots. Additionally, our IP_3R1 immunohistochemical analysis shows that hot spots in general, and branch points in particular, are enriched for IP_3R protein. On the basis of these findings, we conclude that the saltatory propagation of Ca^{2+} waves through hot spots and cold spots in pyramidal neurons derives from a 'fire-diffuse-fire' mechanism of Ca^{2+} wave propagation between IP_3R1 clusters (Pearson & Ponce-Dawson, 1998; Dawson *et al.* 1999). Functionally, we find that the relatively large amplitude of IP_3R-mediated, Ca^{2+} release-associated $[Ca^{2+}]_i$ rises in hot spots and at branch points suggest a singularly important signalling role for Ca^{2+} in these locations. Lastly, we propose that the degree of functional segregation between spatially distinct Ca^{2+}-sensitive dendritic domains may depend on factors that enhance or inhibit the propagation of IP_3R-mediated $[Ca^{2+}]_i$ rises through cold spots.

Several characteristics of hot spots and cold spots indicate that they are not experimental artifacts. (1) Their locations were stable for many individual waves in a given cell, demonstrating that they do not result from random measurement noise. (2) Synaptic stimulation, focal application of an mGluR agonist and focal uncaging of IP_3 all triggered Ca^{2+} waves that propagated through hot spots and cold spots. (3) Locations characterized as hot spots and cold spots during Ca^{2+} waves exhibited uniform, non-propagating, VGCC-mediated rises in $[Ca^{2+}]_i$ in response to suprathreshold depolarization. This finding argues against detection or analysis errors as a source of hot spots and cold spots. (4) Hot and cold spots were observed in Ca^{2+} waves regardless of whether a high- or low-affinity Ca^{2+} dye was used, suggesting that non-uniform Ca^{2+} wave propagation does not result from buffering by Ca^{2+} indicators. (5) The rate of rise of the Ca^{2+} signal in cold spots changed more than did the amplitude. This observation argues against detection errors or analysis errors that might amplify Ca^{2+} signals at hot spots or attenuate them at cold spots, since such a scaling of the Ca^{2+} signal would affect the amplitude and the rate of rise equally. For these reasons, we conclude that the hot spots and cold spots through which Ca^{2+} waves propagate result from spatial variations in the ability of the ER to release Ca^{2+} in response to an IP_3-mobilizing stimulus.

Some of the Ca^{2+} waves we observed propagated in a saltatory fashion for their entire extent, while others propagated in a continuous fashion for most of their extent and were interrupted by just a single cold spot. These observations are consistent with reports that Ca^{2+} waves in individual HeLa cells (Bootman *et al.* 1997) and *Xenopus* oocytes (Callamaras *et al.* 1998) can exhibit both continuous and saltatory propagation. The mode with which Ca^{2+} waves propagate in these non-neuronal cells is thought to be determined primarily by $[IP_3]_i$, such that low $[IP_3]_i$ gives rise to saltatory Ca^{2+} waves while high $[IP_3]_i$ triggers continuously propagating Ca^{2+} waves (Bootman *et al.* 1997; Callamaras *et al.* 1998). These ideas are supported by theoretical studies probing the mechanisms of Ca^{2+} wave propagation. In one such study, the authors found that the amount of IP_3 mobilized within an apical oblique dendrite is a key determinant of the maximum propagation distance of a Ca^{2+} wave away from its initiation site at the apical oblique branch point (Peercy, 2008). In another such study, the authors determined that IP_3-mediated Ca^{2+} release at discrete locations may generate either saltatory Ca^{2+} waves or continuous Ca^{2+} waves. Which kind of Ca^{2+} wave is triggered by a given stimulus depends on three factors: the diffusion constant, the distance between release sites and the duration of Ca^{2+} release at each site (Keizer *et al.* 1995; Pearson & Ponce-Dawson, 1998; Dawson *et al.* 1999). These considerations, as well as numerous other factors including the distribution of Ca^{2+}-binding proteins and the complex structural attributes of neurons, are likely to contribute to the properties of propagating Ca^{2+} waves in pyramidal neurons.

Numerous studies in a variety of cell types have investigated the mechanisms of non-uniform Ca^{2+} wave propagation. In the cell bodies of cultured frog sympathetic neurons, for example, ryanodine receptor-mediated $[Ca^{2+}]_i$ rises are largest in the discrete initiation sites of Ca^{2+} waves. One likely explanation for the non-uniformity of Ca^{2+} release in these cells is the

mean amplitudes of Ca^{2+} signals measured in the leading hot spot of 42 hot spot–cold spot–hot spot sequences, broken down according to whether the Ca^{2+} waves propagated through the cold spot and into the second hot spot (cold spot successes) or whether the Ca^{2+} waves failed in the cold spot (cold spot failures). The amplitudes of internal Ca^{2+} release in the leading hot spot were significantly greater for cold spot successes than they were for cold spot failures. *F*, cumulative probability plots showing the mean rates of rise of Ca^{2+} signals measured in the leading hot spot of 42 hot spot–cold spot–hot spot sequences, broken down according to whether the Ca^{2+} waves propagated through the cold spot and into the second hot spot (cold spot successes) or whether the Ca^{2+} waves failed in the cold spot (cold spot failures). The rates of rise of Ca^{2+} signals in the leading hot spot were significantly greater for cold spot successes than they were for cold spot failures. Statistical significance was determined using Student's paired *t* tests (*$P < 0.001$; **$P < 0.0001$).

distribution of sarco-endoplasmic reticulum Ca^{2+}-ATPase (SERCA) pumps in clusters on the ER membrane. The presence of these clusters raises the possibility that the luminal concentration of Ca^{2+} is non-uniform, and greatest where Ca^{2+} waves initiate (McDonough *et al.* 2000). Non-uniform Ca^{2+} wave propagation much like that we have described here is also seen in cultured astrocytes (Yagodin *et al.* 1994) and oligodendrocytes (Simpson & Russell, 1997). In these cells, both the amplitude and the rate of rise of Ca^{2+} release-associated $[Ca^{2+}]_i$ rises is greatest at sites termed 'focal loci' or 'amplification sites'. Again, Ca^{2+} signalling components, including ryanodine receptors and SERCA pumps, were found to exhibit non-uniform distributions in one or both of these cell types (Simpson & Russell, 1997; Haak *et al.* 2001). Three additional Ca^{2+} signalling components were found to form clusters that were associated with amplification sites. These included the type 2 subtype of IP_3Rs (Sheppard *et al.* 1997), the ER Ca^{2+}-binding protein calreticulin (Simpson *et al.* 1997), and mitochondria (Simpson *et al.* 1997).

Our data support the hypothesis that Ca^{2+} waves in pyramidal neurons may similarly propagate through hot spots and cold spots due to a non-uniform distribution of Ca^{2+} signalling components. More specifically, we found that IP_3R1s form clusters in the primary apical dendrites of hippocampal pyramidal neurons, and that the distribution of distances between IP_3R1 clusters is statistically indistinguishable from the distribution of distances between hot spots. Furthermore, we observed that both clusters of IP_3R1s (Hertle & Yeckel, 2007) and hot spots are frequently located at dendritic branch points. These data suggest that clusters of IP_3R1s may both define the dendritic domains we characterized as hot spots and make those domains more capable of regenerative internal Ca^{2+} release than the cold spot domains flanking them.

The local $[IP_3]_i$ is another factor that may contribute to the existence of hot spots and cold spots. Specifically, hot spots might be more capable of regenerative internal Ca^{2+} release because stimulus-triggered rises in $[IP_3]_i$ reach greater levels at hot spots than at cold spots. Synaptically released glutamate is believed to activate mGluRs situated on the perisynaptic membrane of dendritic spines (Lujan *et al.* 1996), which for pyramidal neurons are found primarily on basal and apical oblique dendrites. Internal Ca^{2+} release and Ca^{2+} waves, however, are predominantly seen in primary apical dendrites (Nakamura *et al.* 2000, 2002; Larkum *et al.* 2003; Power & Sah, 2007). If, as proposed previously (Nakamura *et al.* 2002), IP_3 that is mobilized subsequent to synaptic activation of apical oblique dendrites diffuses to the branch points of those dendrites, then synaptically stimulated rises in $[IP_3]_i$ in the primary apical dendrite would be greatest where oblique dendrites branch from the apical dendritic shaft, and smallest in the sections of dendrite in between. In this light, our observation that hot spots, the locations where IP_3R-dependent $[Ca^{2+}]_i$ rises are greatest, are associated with branch points suggests that Ca^{2+} released at these locations may serve as a kind of intracellular integrator for synaptic activity in nearby oblique dendrites. The additional association we observe between IP_3R1 clusters and branch points could serve to bolster these signals (see also Hertle & Yeckel, 2007).

Importantly, dendritic branch points are enriched not only for IP_3R1s, but also for protein translational machinery (Tiedge & Brosius, 1996) and for Golgi apparatus (Horton & Ehlers, 2004; Horton *et al.* 2005). mGluR stimulation and subsequent IP_3 mobilization have been implicated in the upregulation of postsynaptic protein synthesis (Weiler & Greenough, 1993), which in turn is important for both the maintenance and plasticity of synapses (Sutton & Schuman, 2006). Delivery of membrane lipids and proteins to postsynaptic sites is a prerequisite for these processes, and depends on secretory trafficking mediated by the Golgi apparatus outposts that are found at dendritic branch points (Horton *et al.* 2005). Golgi apparatus-mediated secretory trafficking is modulated by rises in $[Ca^{2+}]_i$ (Burgoyne & Clague, 2003; Wuytack *et al.* 2003). Our observations therefore suggest that mGluR-mediated, IP_3-dependent internal Ca^{2+} release at hot spots may provide an especially important intracellular signal for the growth, maintenance and plasticity of stimulated dendrites and synaptic spines (Tiedge & Brosius, 1996; Horton *et al.* 2005; Dolman & Tepikin, 2006).

Our data are consistent with a 'fire-diffuse-fire' model of Ca^{2+} wave propagation in pyramidal neurons (Keizer *et al.* 1995; Pearson & Ponce-Dawson, 1998; Dawson *et al.* 1999). More specifically, our findings suggest that $[Ca^{2+}]_i$ rises in hot spots result from regenerative, IP_3R-mediated internal Ca^{2+} release, while $[Ca^{2+}]_i$ rises in cold spots result from the diffusion of Ca^{2+} away from branch point release sites. Our data indicate that the successive generation of robust $[Ca^{2+}]_i$ rises at adjacent branch points is likely to depend on the successful diffusion of Ca^{2+} through the cold spots between them. These properties suggest a number of factors that might regulate the degree of functional association or segregation between distinct Ca^{2+}-sensitive dendritic domains. These include the distance between stimulated oblique dendrites, the relative intensity of the stimuli experienced by these dendrites, the subsequent ratio of IP_3-bound to IP_3-unbound IP_3Rs, the filling state of the intracellular Ca^{2+} pool, and the cytosolic Ca^{2+} buffering capacity.

Ca^{2+} waves are part of a growing list of mechanisms that produce compartmentalized $[Ca^{2+}]_i$ increases in dendrites. These mechanisms include IP_3R-mediated Ca^{2+} release in Purkinje neurons (Finch & Augustine, 1998; Takechi *et al.* 1998), NMDA receptor-mediated Ca^{2+} spikes in cortical pyramidal neurons (Schiller *et al.* 2000), and

NMDA receptor- and VGCC-mediated Ca^{2+} spikes in hippocampal CA1 pyramidal neurons (Golding *et al.* 2002). The dendrites in which we have studied Ca^{2+} waves contain voltage-gated K^+ (Hoffman *et al.* 1997) and Ca^{2+} channels (Magee & Johnston, 1995) that are regulated by Ca^{2+}-dependent mechanisms (Brehm & Eckert, 1978; Peterson *et al.* 1999; Liang *et al.* 2003; Goo *et al.* 2006). A number of studies have implicated the $[Ca^{2+}]_i$ rises associated with internal Ca^{2+} release and Ca^{2+} waves in the regulation of pyramidal neuronal excitability via either the activation and/or inhibition of Ca^{2+}-dependent currents (Yamamoto *et al.* 2002; Stutzmann *et al.* 2003; Gulledge & Kawaguchi, 2007; Hagenston *et al.* 2008). Thus, the diffusional barrier imposed by cold spots and the factors which regulate hot spot associativity, insofar as they may function to limit or enhance the extent of Ca^{2+} wave propagation, may control all of the intensity, the spatial distribution, and the uniformity of Ca^{2+}-dependent changes in dendritic and neuronal excitability.

References

Augustine GJ, Santamaria F & Tanaka K (2003). Local calcium signaling in neurons. *Neuron* **40**, 331–346.

AVMA Panel on Euthanasia. American Veterinary Medical Association (2001). 2000 Report of the AVMA Panel on Euthanasia. *J Am Vet Med Assoc* **218**, 669–696.

Benhassine N & Berger T (2005). Homogeneous distribution of large-conductance calcium-dependent potassium channels on soma and apical dendrite of rat neocortical layer 5 pyramidal neurons. *Eur J Neurosci* **21**, 914–926.

Berridge MJ (1997). Elementary and global aspects of calcium signalling. *J Physiol* **499**, 291–306.

Berridge MJ (1998). Neuronal calcium signaling. *Neuron* **21**, 13–26.

Berridge MJ (2006). Calcium microdomains: organization and function. *Cell Calcium* **40**, 405–412.

Berridge MJ, Lipp P & Bootman MD (2000). The versatility and universality of calcium signalling. *Nat Rev Mol Cell Biol* **1**, 11–21.

Bezprozvanny I, Watras J & Ehrlich BE (1991). Bell-shaped calcium-response curves of $Ins(1,4,5)P_3$- and calcium-gated channels from endoplasmic reticulum of cerebellum. *Nature* **351**, 751–754.

Bootman M, Niggli E, Berridge M & Lipp P (1997). Imaging the hierarchical Ca^{2+} signalling system in HeLa cells. *J Physiol* **499.2**, 307–314.

Boulware MJ & Marchant JS (2005). IP_3 receptor activity is differentially regulated in endoplasmic reticulum subdomains during oocyte maturation. *Curr Biol* **15**, 765–770.

Brehm P & Eckert R (1978). Calcium entry leads to inactivation of calcium channel in *Paramecium. Science* **202**, 1203–1206.

Burgoyne RD & Clague MJ (2003). Calcium and calmodulin in membrane fusion. *Biochim Biophys Acta* **1641**, 137–143.

Callamaras N, Marchant JS, Sun XP & Parker I (1998). Activation and co-ordination of $InsP_3$-mediated elementary Ca^{2+} events during global Ca^{2+} signals in *Xenopus* oocytes. *J Physiol* **509**, 81–91.

Callamaras N & Parker I (1998). Caged inositol 1,4,5-trisphosphate for studying release of Ca^{2+} from intracellular stores. *Methods Enzymol* **291**, 380–403.

Cheng H, Lederer MR, Lederer WJ & Cannell MB (1996). Calcium sparks and $[Ca^{2+}]_i$ waves in cardiac myocytes. *Am J Physiol Cell Physiol* **270**, C148–159.

Cheng H, Lederer WJ & Cannell MB (1993). Calcium sparks: elementary events underlying excitation-contraction coupling in heart muscle. *Science* **262**, 740–744.

Dawson SP, Keizer J & Pearson JE (1999). Fire-diffuse-fire model of dynamics of intracellular calcium waves. *Proc Natl Acad Sci U S A* **96**, 6060–6063.

Dolman NJ & Tepikin AV (2006). Calcium gradients and the Golgi. *Cell Calcium* **40**, 505–512.

Finch EA & Augustine GJ (1998). Local calcium signalling by inositol-1,4,5-trisphosphate in Purkinje cell dendrites. *Nature* **396**, 753–756.

Finch EA, Turner TJ & Goldin SM (1991). Calcium as a coagonist of inositol 1,4,5-trisphosphate-induced calcium release. *Science* **252**, 443–446.

Gipson KE & Yeckel MF (2007). Coincident glutamatergic and cholinergic inputs transiently depress glutamate release at rat Shaffer collateral synapses. *J Neurophysiol* **97**, 4108–4119.

Golding NL, Staff NP & Spruston N (2002). Dendritic spikes as a mechanism for cooperative long-term potentiation. *Nature* **418**, 326–331.

Goo YS, Lim W & Elmslie KS (2006). Ca^{2+} enhances U-type inactivation of N-type (CaV2.2) calcium current in rat sympathetic neurons. *J Neurophysiol* **96**, 1075–1083.

Gulledge AT & Kawaguchi Y (2007). Phasic cholinergic signaling in the hippocampus: functional homology with the neocortex? *Hippocampus* **17**, 327–332.

Haak LL, Song LS, Molinski TF, Pessah IN, Cheng H & Russell JT (2001). Sparks and puffs in oligodendrocyte progenitors: cross talk between ryanodine receptors and inositol trisphosphate receptors. *J Neurosci* **21**, 3860–3870.

Hagenston AM, Fitzpatrick JS & Yeckel MF (2008). mGluR-mediated calcium waves that invade the soma regulate firing in layer V medial prefrontal cortical pyramidal neurons. *Cereb Cortex* **18**, 407–423.

Hertle DN & Yeckel MF (2007). Distribution of inositol-1,4,5-trisphosphate receptor isotypes and ryanodine receptor isotypes during maturation of the rat hippocampus. *Neuroscience* **150**, 625–638.

Hoffman DA, Magee JC, Colbert CM & Johnston D (1997). K^+ channel regulation of signal propagation in dendrites of hippocampal pyramidal neurons. *Nature* **387**, 869–875.

Hong M & Ross WN (2007). Priming of intracellular calcium stores in rat CA1 pyramidal neurons. *J Physiol* **584**, 75–87.

Horton AC & Ehlers MD (2004). Secretory trafficking in neuronal dendrites. *Nat Cell Biol* **6**, 585–591.

Horton AC, Racz B, Monson EE, Lin AL, Weinberg RJ & Ehlers MD (2005). Polarized secretory trafficking directs cargo for asymmetric dendrite growth and morphogenesis. *Neuron* **48**, 757–771.

Iino M (1990). Biphasic Ca^{2+} dependence of inositol 1,4,5-trisphosphate-induced Ca release in smooth muscle cells of the guinea pig taenia caeci. *J Gen Physiol* **95**, 1103–1122.

Jaffe DB & Brown TH (1994). Metabotropic glutamate receptor activation induces calcium waves within hippocampal dendrites. *J Neurophysiol* **72**, 471–474.

Kapur A, Yeckel M & Johnston D (2001). Hippocampal mossy fiber activity evokes Ca^{2+} release in CA3 pyramidal neurons via a metabotropic glutamate receptor pathway. *Neuroscience* **107**, 59–69.

Keizer J, Li YX, Stojilkovic S & Rinzel J (1995). $InsP_3$-induced Ca^{2+} excitability of the endoplasmic reticulum. *Mol Biol Cell* **6**, 945–951.

Larkum ME, Watanabe S, Nakamura T, Lasser-Ross N & Ross WN (2003). Synaptically activated Ca^{2+} waves in layer 2/3 and layer 5 rat neocortical pyramidal neurons. *J Physiol* **549**, 471–488.

Liang H, DeMaria CD, Erickson MG, Mori MX, Alseikhan BA & Yue DT (2003). Unified mechanisms of Ca^{2+} regulation across the Ca^{2+} channel family. *Neuron* **39**, 951–960.

Lujan R, Nusser Z, Roberts JD, Shigemoto R & Somogyi P (1996). Perisynaptic location of metabotropic glutamate receptors mGluR1 and mGluR5 on dendrites and dendritic spines in the rat hippocampus. *Eur J Neurosci* **8**, 1488–1500.

McDonough SI, Cseresnyes Z & Schneider MF (2000). Origin sites of calcium release and calcium oscillations in frog sympathetic neurons. *J Neurosci* **20**, 9059–9070.

Magee JC & Johnston D (1995). Characterization of single voltage-gated Na^+ and Ca^{2+} channels in apical dendrites of rat CA1 pyramidal neurons. *J Physiol* **487**, 67–90.

Marchant JS & Taylor CW (1997). Cooperative activation of IP_3 receptors by sequential binding of IP_3 and Ca^{2+} safeguards against spontaneous activity. *Curr Biol* **7**, 510–518.

Morikawa H, Khodakhah K & Williams JT (2003). Two intracellular pathways mediate metabotropic glutamate receptor-induced Ca^{2+} mobilization in dopamine neurons. *J Neurosci* **23**, 149–157.

Nakamura T, Barbara JG, Nakamura K & Ross WN (1999). Synergistic release of Ca^{2+} from IP_3-sensitive stores evoked by synaptic activation of mGluRs paired with backpropagating action potentials. *Neuron* **24**, 727–737.

Nakamura T, Lasser-Ross N, Nakamura K & Ross WN (2002). Spatial segregation and interaction of calcium signalling mechanisms in rat hippocampal CA1 pyramidal neurons. *J Physiol* **543**, 465–480.

Nakamura T, Nakamura K, Lasser-Ross N, Barbara JG, Sandler VM & Ross WN (2000). Inositol 1,4,5-trisphosphate (IP_3)-mediated Ca^{2+} release evoked by metabotropic agonists and backpropagating action potentials in hippocampal CA1 pyramidal neurons. *J Neurosci* **20**, 8365–8376.

Ngo-Anh TJ, Bloodgood BL, Lin M, Sabatini BL, Maylie J & Adelman JP (2005). SK channels and NMDA receptors form a Ca^{2+}-mediated feedback loop in dendritic spines. *Nat Neurosci* **8**, 642–649.

Oberdorf J, Vallano ML & Wojcikiewicz RJ (1997). Expression and regulation of types I and II inositol 1,4,5-trisphosphate receptors in rat cerebellar granule cell preparations. *J Neurochem* **69**, 1897–1903.

Parker I, Choi J & Yao Y (1996). Elementary events of $InsP_3$-induced Ca^{2+} liberation in *Xenopus* oocytes: hot spots, puffs and blips. *Cell Calcium* **20**, 105–121.

Parker I & Ivorra I (1990). Localized all-or-none calcium liberation by inositol trisphosphate. *Science* **250**, 977–979.

Pearson JE & Ponce-Dawson S (1998). Crisis on skid row. *Physica A* **257**, 141–148.

Peercy BE (2008). Initiation and propagation of a neuronal intracellular calcium wave. *J Comput Neurosci* **25**, 334–348.

Peterson BZ, DeMaria CD, Adelman JP & Yue DT (1999). Calmodulin is the Ca^{2+} sensor for Ca^{2+}-dependent inactivation of L-type calcium channels. *Neuron* **22**, 549–558.

Power JM & Sah P (2002). Nuclear calcium signaling evoked by cholinergic stimulation in hippocampal CA1 pyramidal neurons. *J Neurosci* **22**, 3454–3462.

Power JM & Sah P (2005). Intracellular calcium store filling by an L-type calcium current in the basolateral amygdala at subthreshold membrane potentials. *J Physiol* **562**, 439–453.

Power JM & Sah P (2007). Distribution of IP_3-mediated calcium responses in basolateral amygdala neurons and their role in nuclear signalling. *J Physiol* **580**, 835–57.

Pozzo-Miller LD, Petrozzino JJ, Golarai G & Connor JA (1996). Ca^{2+} release from intracellular stores induced by afferent stimulation of CA3 pyramidal neurons in hippocampal slices. *J Neurophysiol* **76**, 554–562.

Raymond CR & Redman SJ (2006). Spatial segregation of neuronal calcium signals encodes different forms of LTP in rat hippocampus. *J Physiol* **570**, 97–111.

Rose CR & Konnerth A (2001). Stores not just for storage. Intracellular calcium release and synaptic plasticity. *Neuron* **31**, 519–522.

Schiller J, Major G, Koester HJ & Schiller Y (2000). NMDA spikes in basal dendrites of cortical pyramidal neurons. *Nature* **404**, 285–289.

Sharp AH, Nucifora FC Jr, Blondel O, Sheppard CA, Zhang C, Snyder SH, Russell JT, Ryugo DK & Ross CA (1999). Differential cellular expression of isoforms of inositol 1,4,5-triphosphate receptors in neurons and glia in brain. *J Comp Neurol* **406**, 207–220.

Sheppard CA, Simpson PB, Sharp AH, Nucifora FC, Ross CA, Lange GD & Russell JT (1997). Comparison of type 2 inositol 1,4,5-trisphosphate receptor distribution and subcellular Ca^{2+} release sites that support Ca^{2+} waves in cultured astrocytes. *J Neurochem* **68**, 2317–2327.

Shuai J, Rose HJ & Parker I (2006). The number and spatial distribution of IP_3 receptors underlying calcium puffs in *Xenopus* oocytes. *Biophys J* **91**, 4033–4044.

Simpson PB, Mehotra S, Lange GD & Russell JT (1997). High density distribution of endoplasmic reticulum proteins and mitochondria at specialized Ca^{2+} release sites in oligodendrocyte processes. *J Biol Chem* **272**, 22654–22661.

Simpson PB & Russell JT (1997). Role of sarcoplasmic/endoplasmic-reticulum Ca^{2+}-ATPases in mediating Ca^{2+} waves and local Ca^{2+}-release microdomains in cultured glia. *Biochem J* **325**, 239–247.

Stutzmann GE, LaFerla FM & Parker I (2003). Ca^{2+} signaling in mouse cortical neurons studied by two-photon imaging and photoreleased inositol triphosphate. *J Neurosci* **23**, 758–765.

Sun XP, Callamaras N, Marchant JS & Parker I (1998). A continuum of InsP_3-mediated elementary Ca^{2+} signalling events in *Xenopus* oocytes. *J Physiol* **509**, 67–80.

Sutton MA & Schuman EM (2006). Dendritic protein synthesis, synaptic plasticity, and memory. *Cell* **127**, 49–58.

Takechi H, Eilers J & Konnerth A (1998). A new class of synaptic response involving calcium release in dendritic spines. *Nature* **396**, 757–760.

Tateishi Y, Hattori M, Nakayama T, Iwai M, Bannai H, Nakamura T, Michikawa T, Inoue T & Mikoshiba K (2005). Cluster formation of inositol 1,4,5-trisphosphate receptor requires its transition to open state. *J Biol Chem* **280**, 6816–6822.

The National Academies Institute for Laboratory Animal Research (2003). *Guidelines for the Care and Use of Mammals in Neuroscience and Behavioral Research*. The National Academies Press, Washington, DC.

Tiedge H & Brosius J (1996). Translational machinery in dendrites of hippocampal neurons in culture. *J Neurosci* **16**, 7171–7181.

Wang SS & Thompson SH (1995). Local positive feedback by calcium in the propagation of intracellular calcium waves. *Biophys J* **69**, 1683–1697.

Weiler IJ & Greenough WT (1993). Metabotropic glutamate receptors trigger postsynaptic protein synthesis. *Proc Natl Acad Sci U S A* **90**, 7168–7171.

Wuytack F, Raeymaekers L & Missiaen L (2003). PMR1/SPCA Ca^{2+} pumps and the role of the Golgi apparatus as a Ca^{2+} store. *Pflugers Arch* **446**, 148–153.

Xia XM, Fakler B, Rivard A, Wayman G, Johnson-Pais T, Keen JE, Ishii T, Hirschberg B, Bond CT, Lutsenko S, Maylie J & Adelman JP (1998). Mechanism of calcium gating in small-conductance calcium-activated potassium channels. *Nature* **395**, 503–507.

Yagodin SV, Holtzclaw L, Sheppard CA & Russell JT (1994). Nonlinear propagation of agonist-induced cytoplasmic calcium waves in single astrocytes. *J Neurobiol* **25**, 265–280.

Yamamoto K, Nakano M, Hashimoto K, Shimohama S & Kato N (2002). Emergence of a functional coupling between inositol-1,4,5-trisphosphate receptors and calcium channels in developing neocortical neurons. *Neuroscience* **109**, 677–685.

Yao Y, Choi J & Parker I (1995). Quantal puffs of intracellular Ca^{2+} evoked by inositol trisphosphate in *Xenopus* oocytes. *J Physiol* **482**, 533–553.

Yeckel MF, Kapur A & Johnston D (1999). Multiple forms of LTP in hippocampal CA3 neurons use a common postsynaptic mechanism. *Nat Neurosci* **2**, 625–633.

Yus-Najera E, Santana-Castro I & Villarroel A (2002). The identification and characterization of a noncontinuous calmodulin-binding site in noninactivating voltage-dependent KCNQ potassium channels. *J Biol Chem* **277**, 28545–28553.

Acknowledgements

Funded by the Whitehall Foundation, the Kavli Foundation, the Dart Foundation, NIMH (ROI-MH067830 and P50-MH068789) (MFY), and the NSF Graduate Research Fellowship (AWH).

Authors' present addresses

A. M. Hagenston: Institute of Neurobiology, Ruprecht-Karls University of Heidelberg, Germany.
D. N. Hertle: Department of Neurosurgery, Ruprecht-Karls University of Heidelberg, Germany.